Tunable electronic and magnetic properties of Graphene/1T-$CrTe_2$ van der Waals heterostructure: A first-principles analysis

A Thesis

submitted in partial fulfillment for the Degree of

MASTER OF SCIENCE

as a part of Integrated Ph.D. programme in

MATERIALS SCIENCE

by

Surabhi Menon

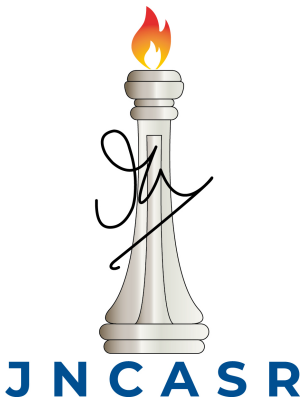

CHEMISTRY AND PHYSICS OF MATERIALS UNIT,
JAWAHARLAL NEHRU CENTRE FOR ADVANCED SCIENTIFIC RESEARCH
Bangalore - 560 064

MARCH, 2022

To my family

DECLARATION

I hereby declare that the matter embodied in the thesis entitled "**Tunable electronic and magnetic properties of Graphene/1T-$CrTe_2$ van der Waals heterostructure: A first-principles analysis**" is the result of investigations carried out by me at the Chemistry and Physics of Materials Unit, Jawaharlal Nehru Centre for Advanced Scientific Research, Bangalore, India under the supervision of Prof. Umesh V. Waghmare and that it has not been submitted elsewhere for the award of any degree or diploma.

In keeping with the general practice in reporting scientific observations, due acknowledgement has been made whenever the work described is based on the findings of other investigators.

Surabhi Menon

CERTIFICATE

I hereby certify that the matter embodied in this thesis entitled "**Tunable electronic and magnetic properties of Graphene/1T-$CrTe_2$ van der Waals heterostructure: A first-principles analysis** " has been carried out by Ms. Surabhi Menon at the Chemistry and Physics of Materials Unit, Jawaharlal Nehru Centre for Advanced Scientific Research, Bangalore, India under my supervision and that it has not been submitted elsewhere for the award of any degree or diploma.

Prof. Umesh V. Waghmare

(Research Supervisor)

Acknowledgment

First of all I want to express my sincere and heartfelt gratitude to my supervisor Prof. Umesh V. Waghmare to whom I owe deepest gratitude for his constant support and excellent guidance. His valuable comments and instructions in preparing presentations, seminars and writing papers have helped me immensely. I am extremely grateful for having invaluable scientific and non-scientific discussions with Prof. Waghmare, which have always motivated me to follow scientific ideas, work on them diligently and to solve them. His passion for science has always motivated me. I am very thankful for his kindness and encouragement throughout my MS thesis.

I am thankful to all my past and present lab members of Materials Theory Group who have helped me in several ways and for scientific discussions during lab meetings and otherwise, by which I have learned a lot. I thank Dr. Lakshay, Dr. Meghna, Dr. Meha, Dr. Prasad, Dr. Durgesh, Dr. Arpita Paul, Dr. Arpita Sen, Narendra, Koyendrila, Raagya, Shashank, Arijit, Sarbajit, Bhuvaneswari, Mohit for academic, non-academic and fun interactions.

I would like to sincerely thank Prof. C.N.R Rao, FRS for his support and inspiration. I am thankful to Prof. A. Sundaresan, Prof. Rajesh Ganapathy, Prof. S. Balasubramanian, Prof. T. K. Maji, Prof. N. S. Vidhyadiraja, Prof. U. V. Waghmare, Prof. S. Narasimhan, Prof. K. S. Narayan, Prof. M. Eswaramoorthy, Dr. Bivas Saha, Dr. Sarit Agasti, Dr. Premkumar Senguttuvan, Prof. Chandrabhas Narayana, Prof. Subir K. Das, Prof. Sridhar Rajaram, Prof. Meher Prakash, Prof. Ranjan Datta, Prof. Kavita Jain, Prof. A. Chakraborty (IISc), Dr. Diwakar S. Venkatesan, Dr. Krishna Prasad (CeNS) for their excellent courses which were interesting and enlightening.

I thank Int. PhD. coodinators Prof. Rajesh Ganapathy and Prof. Kavita Jain for their support and Mr. Ala Srinivas Rao for help with instruments and measurements.

I am grateful to my Integrated Ph.D. batch-mates Uttam, Aashish, Dipanjana, Sohini, Animesh, Tarak, Arif for all their support and for making my hostel life enjoyable. I appreciate all the advice and guidance from my Ph.D. seniors and Integrated Ph.D. seniors.

I express my sincere gratitude to Aruna Ma'am and Kruti for their warm hospitality, affection and support during our group treats.

I acknowledge the support from staffs at academic, administrative, security, Dhanvantri, library, and comp lab. I also thank Hostel office, Hostel mess, Chandraya and utility stores for making life in JNCASR comfortable and easy. I would like to acknowledge the Centre for Computational Material Science (CCMS), JNCASR for the computational facilities.

I am thankful to my teachers in school and college and special thanks to Dr. Alka Vohra, Dr. Manoj Kumar , Bharat who motivated me to pursue higher studies.

I am grateful to have met amazing people in JNC who have always believed in me and made my journey in JNC memorable so far. I thank Yashwini, Pragya, Aneeta, Rahul, Sudip, Aditya, Anustup, Amit, Sakshi, Deeksha. I feel blessed to have friends like Yogita, Surbhi, Gyanvi, Anushkar, Prabhat, Joshi and I thank them for their unconditional love and support. I am thankful to Gayatri, Renjith, Vaishnavi, Sushant, Ruchi, Chandan. Their company made me feel comfortable in this new city.

Lastly, I thank my parents, my brother Suraj and Malavika *chechi* for always believing in me, providing me endless freedom and unconditional support at all stages of my life.

Synopsis

Since the discovery of graphene, 2D materials have attracted substantial attention due to their interesting physical and chemical features as well as their potential device applications. Various 2D materials have been predicted and discovered from semimetal, semiconductor, insulator to conductors. In comparison to bulk materials, the current research on 2D materials and their devices is focused on the growth of single 2D materials and the exploration of devices based on heterostructures created by stacking one layer of 2D material on another. The growth of a van der Waals heterostructure usually occurs by layering one material on top of another, and thus has unique properties not seen in single materials. For example heterstructure constructured by stacking magnetic and non-magnetic material, the magnetic proximity effect comes into play, significantly changing the heterostructures' electronic and magnetic properties. More interesting phenomena kick in when external perturbations are applied and may lead to the appearance of material-specific effects. In this thesis, we use density functional theory (DFT) to study the electronic and magnetic properties of van der Waals heterostructure created by graphene and monolayer of 1T-$CrTe_2$. Chapter 1 of this thesis introduces a brief introduction to the theme of this thesis. Chapter 2 discusses the methods and formalism used in our calculations. Chapter 3 explores the electronic and magnetic properties and studies the effect of carrier doping (holes and electrons) on the electronic and magnetic properties of Graphene/1T-$CrTe_2$ heterostructure. We examine the effect of applying perpendicular external positive and negative electric fields along z-direction on the magnetization and polarization in the heterostructure. Due to the breaking of symmetries and plausible variation in magnetization and polarization,

the magnetoelectric coupling is also investigated in this thesis. Furthermore, the coupling of strain with magnetism and the intrinsic electric field is examined. Simulations using density functional theory have thus proven to be effective for selecting materials for a given application based on concerns of cost and performance and understanding the limitations of materials.

List of Publications

1. "First-principles analysis of tunable electronic and magnetic properties of Graphene and monolayer ferromagnetic 1T-$CrTe_2$ van der Waals heterostructure", Surabhi Menon and Umesh V. Waghmare, (manusript under preparation).

List of Figures

List of Tables

Contents

Chapter 1

Introduction

Materials science involves combination of ideas from several fields of research such as physics, chemistry, biology and engineering. Understanding material behavior such as electronic, mechanical, magnetic, optical, chemical and thermal properties help bring new insights into interesting problems in science and research. Materials are enablers in unlocking applications in electronics, energy, space technology, metallurgy, nanotechnology, etc.

Materials modeling or simulation of materials is one of the powerful methods to understand and study the properties of materials, starting from macroscopic objects to microscopic details such as electrons and nuclei. Mathematical models can investigate complex problems and help in understanding how material structures govern its properties and also complement the experiments. The development of advanced and new materials such as semiconductors in nanotechnology, energy materials, soft materials, liquid crystals, and biomaterials aid in eradicating challenges faced by today's modern world.

As a result of high-throughput schemes, we obtain a large number of theoretical and experimental data, a logical next step is the use and development of novel tools capable of extracting knowledge from such data. Density Functional Theory (DFT) is powerful computational quantum mechanical tool to solving and understanding properties of the many-body systems, in particlar condensed phases, molecules, atoms and is used in various fields such as physics,

chemistry, biology, and materials science. The first-principles approach can be used to estimate the physical properties of a material such as electronic structure [1], stress, elastic constants, polarisation, optical and vibrational properties, with high precision. We can describe a quantum mechanical system as a set of atomic nuclei and electrons interacting via coulombic and electrostatic forces [2]. All the properties can be derived by solving time independent Schrödinger's equation.

$$\hat{H}\Psi_n(R,r) = \varepsilon_n\Psi_n(R,r) \tag{1.1}$$

where ε_n are the energy eigenvalues and Ψ_n(R,r) are the corresponding eigenfunctions, which must be antisymmetric with respect to exchange of electronic coordinates r and symmetric or antisymmetric with respect to exchange of coordinates of nuclei R.

In Density Functional Theory, many electron equations are mapped onto a set of effective equations for one electron. Alternatively, classical atomistic simultions like Monte Carlo methods can be used to study the properties of materials longer length scales. This thesis focuses to explore properties of a van der Waals heterostructure created using Graphene and monolayer ferromagnetic 1T-$CrTe_2$, and its response to external perturbations, such as electric field, carrier doping, and strain.

1.1 Two-dimensional materials

Since the first realization of Graphene in 2004, two-dimensional materials have attracted great interest due to their unique properties and applications such as optoelectronics, flexible electronics, sensors, solar cells and supercapacitors. It consists of single or few layers of atoms. To understand and study several interesting phenomena in materials science and predictions of new 2D materials, Density Functional Theory (DFT) plays a crucial role. Due to its extraordinary properties, such as electronic, thermal, and mechanical properties, graphene [3] is among the most remarkable nanomaterials. The developments in the research in graphene stimulates research interests on 2D materials. There have been several experimental realizations of other

2D materials such as MoS_2 [4], hexagonal boron nitride [5].

It was predicted by theorists that there would be disintegration of low dimensional crystals [6] at finite temperature because of thermal fluctuations due to significant displacements of lattice atoms. These displacements were considered to be of the same order as the material's interatomic distance. Later, Mermin built on this theory [7], followed by evidence from the experimental observation that with the reduction in thickness of film, the melting points of thin films rapidly decrease [8]. In the past years, analogous materials to Graphene have been synthesized such as borophene [9], phosphorene [10], germanene [11], stanene [12], antimonene [13]. These 2D materials have similar structure, but have properties different from graphene. Graphene has zero band gap and shows metallicity, whereas materials like MoS_2, VSe_2, h-BN, WSe_2, have direct band gaps, which makes them favourable materials for phototransistors, energy storage, optical devices, and sensors [14–16]. Apart from these, stanene is theoretically predicted to be a 2D topological insulator, which exhibits superconductivity at the edges [17]. The electronic, optical, thermal, and magnetic properties determine the potential applications of 2D materials in manufacturing and engineering. The majority of the 2D materials being investigated belong to the broader class of layered materials.

1.1.1 Layered materials

Layered materials are made of two-dimensional sheets formed of a single layer of atoms or polyhedra layer thick, firmly bonded covalently or ionically within each layer but weakly bonded by van der Waals forces to adjacent layers. Usual approaches for obtaining single layer thick 2D materials from these solids are mechanical exfoliation using 'Scotch tape', chemical exfoliation by dispersing in a solvent with suitable surface tension [18]. Mechanical exfoliation is considered as less destructive method and has been used to create large, 10 μm single-layer flakes on substrates. 2D layered crystals which are well known include transition metal dichalcogenides [19], nitrides [20], and transition metal oxides [21]. Especially, the transition metal dichalcogenides exhibit a wide range of electronic, optical, mechanical, chemical, and thermal properties. For

example, WTe_2 shows anomalous giant magnetoresistance and superconductivity [22]. Transition metal dichalcogenide (TMD) monolayers are layered materials of type AX_2, with A as transition metal atom and X as chalcogen atom. Layer of A atoms are sandwiched between two layers of X atoms. Properties of these materials range from semiconducting, metallic, ferromagnetic, superconducting, depending on the atomic coordination of transition metal and the number of electrons present in the d-orbitals [23]. 2D layered materials show diverse and interesting properties in the bulk. Isolating sp^2 bonded graphene from bulk graphite led to some extraordinary properties of graphene, suggesting that monolayer of nongraphene 2D materials may also have unique properties which may differ from their bulk properties. Layered chalcogenide materials such as Bi_2Se_3 and Bi_2Te_3, have attracted considerable attention for being topological insulators due to their unique electronic and thermal properties. Recently, studies on 2D magnetic materials have provided a unique platform for exploring the microscopic origins of magnetic ordering in low dimensions.

1.1.2 Two-dimensional magnetic materials

A key feature of magnetism is the orderly arrangement of magnetic moments over macroscopic scales, with the spontaneous breaking of time-reversal symmetry. 2D magnetic materials are 2D materials that exhibit some order such as antiferromagnetism or ferromagnetism. Interactions between neighboring spins lead to specific relative orientations between them. At zero temperature, this local order can extend upto larger length scales. With increased temperature, thermal fluctuations tend to disturb the orientation of magnetic moments, which destroys the long-range order above T_c. The dimensionality plays an essential role in understanding the impact of thermal fluctuations on the critical behavior of systems [24]. In bulk case, magnetic phase transition can occur at finite temperature, whereas in one-dimensional case, long-range order is possible only at zero temperature [25]. It is more complex in 2D materials.

Magnetism in two-dimensional materials was first observed with the exfoliation of monolayer and few-layer of $FePS_3$ [26] and $CrSiTe_3$ [27]. The first explicit experimental confirmation of

magnetism occurred in 2017 by researchers in atomically thin CrI_3 [28] and $Cr_2Ge_2Te_6$ [29]. Since then magnetic order was also observed in single atomic layers of VSe_2 [30], Fe_3GeTe_2 [31] and $MnSe_2$ [32].

1.2 van der Waals heterostructure

2D crystals have remarkable properties, but the most tremendous potential lies in stacking 2D layers together to form hybrid multilayer heterostructures. Due to weak van der Waals forces, such heterostructures are called van der Waals heterostructures (vdWHs). Heterostructures are made by stacking 2D crystals on top of each other. For example, by taking a monolayer and putting it on top of another monolayer or few layer crystal. The resulting stack represents an artificial material. The in-plane stability of 2D crystals is due to strong covalent bonds and weak van der Waals force, sufficient to keep the stack altogether. The possibility of experimentally realizing multilayer van der Waals heterostructures has been demonstrated recently [33, 34]. It gives rise to exciting possibilities for controlling the transport of charge carriers, phonons, and photons within the interfaces and designing novel devices for engineering applications.

When stacking 2D materials into heterostructures, an important consideration is the crystal orientation. The alignment of the lattice can have a notable impact on the structural effects on systems such as moiré pattern, that might result in commensurate or incommensurate transition. The commensurate state corresponds to the regions with matching lattice constants and incommensurate state corresponds to the regions with significant lattice mismatch, where the elastic energy is considerable compared to van der Waals energy [35].

1.3 Magnetic Proximity Effect

Magnetic proximity effects in heterostructures are crucial to exploring and manipulating phenomena sensitive to interfacial properties such as spintronics, topological properties, supercon-

ducting, etc. The recent inception of 2D magnetic materials have opened up new prospectives in exploring proximity effect in heterostructures [28]. It is usually a short-range effect because the extension of the electronic wavefunctions over the interface is finite. Therefore, van der Waals materials serve as a platform to realize and harness proximity effect [36].

A material acquires properties of its neighbors through the proximity effect, becoming magnetic, superconducting, topologically nontrivial, etc. For example, in heterostructures formed by monolayer WSe_2 and atomically thin CrI_3, valley Zeeman splitting of about 3 meV at zero applied magnetic field is observed below the Curie temperature, equivalent to an effective magnetic field of about 13 T [37]. Such large induced exchange fields are promising for realizing magnetic proximity effects that modify the properties of materials adjacent to the magnetic material. Stacking one material on another magnetic vdW material leads to atomically sharp interfaces that allow for consistent proximity coupling [38].

1.3.1 Magnetoelectric coupling

The magnetoelectric coupling denoted coupling between the magnetic and the electronic properties of materials. The first example of magnetoelectric effect was described by Wilhelm Röntgen [39] in 1888, who observed that where an intrinsic linear magnetoelectric effect was predicted theoretically and later confirmed experimentally is Cr_2O_3 [40]. The magnetoelectric effect is prevalent in multiferroic materials [41]. The contribution to ME can be obtained in the presence of electric fields by the Landau theory of free energy expansion of the material given by,

$$F(\vec{E},\vec{H}) = F_0 - P_i^s E_i - M_i^s H_i - \frac{1}{2}\epsilon_0\epsilon_{ij}E_iE_j - \frac{1}{2}\mu_0\mu_{ij}H_iH_j - \alpha_{ij}E_iH_j - ... \qquad (1.2)$$

where $\vec{E}$ and $\vec{H}$ as electric field and magnetic field respectively. $\vec{P}^s$ and $\vec{M}^s$ are spontaneous polarization and magnetization respectively, whereas ϵ and μ are electric and magnetic

susceptibilities. Electric polarization can be obtained by differentiating (2)

$$\vec{P}_i(\vec{E},\vec{H}) = -\frac{\partial F}{\partial E_i} \tag{1.3}$$

$$\vec{P}_i(\vec{E},\vec{H}) = P_i^s + \frac{1}{2}\epsilon_0\epsilon_{ij}E_j + \alpha_{ij}H_j \tag{1.4}$$

and magnetization

$$\vec{M}_i(\vec{E},\vec{H}) = -\frac{\partial F}{\partial H_i} \tag{1.5}$$

$$\vec{M}_i(\vec{E},\vec{H}) = M_i^s + \frac{1}{\mu_0}\mu_{ij}H_j + \frac{1}{\mu_0}\alpha_{ij}E_i \tag{1.6}$$

$\vec{P}^s$ and $\vec{M}^s$ are spontaneous polarization and magnetization, respectively, whereas ϵ and μ are electric and magnetic susceptibilities. $\vec{E}$ and $\vec{H}$ as electric field and magnetic field, respectively. The tensor α_{ij} corresponds to induction of polarization by a magnetic field or magnetization by an electric field, which is identified as the linear ME effect. It is complemented by higher-order ME effects parametrized by the tensors β and γ [42].

1.3.2 Piezoelectric effect

Piezoelectric Effect is the ability of materials to generate an electric field in response to applied mechanical stress. The piezoelectric effect was first seen in 1880 by Jacques and Pierre Curie [43]. The piezoelectric effect results from the linear electromechanical interaction between crystalline materials' mechanical and electrical states with no inversion symmetry. When piezoelectric material is placed under mechanical stress, there occurs reconfiguration of the dipole-inducing surrounding or re-orientation of molecular dipole moments. The inverse piezoelectric effect was deduced from the principles of thermodynamics by Lippman [44]. When the reverse effect is taken into consideration, an external electrical field either stretches or compresses the piezoelectric material. This effect has many applications such as sensors in the medical field, microphones, sound detection, heating devices, ignition of gas stove, etc. The piezoelectric

effect forms the basis for scanning probe microscopes that resolve images at the scale of atoms. These effects are firmly dependent on the crystal orientation concerning the strain. In many cases, a robust piezoelectric effect is observed in one direction. The direction of polarization, also known as poling axis, is parallel to the z-axis. According to the standard notation, the x,y, and z axes correspond to subscripts 1,2, and 3, respectively.

The electrical behaviour of piezoelectric materials can be described by Hooke's law as [45]

$$D = \varepsilon E \tag{1.7}$$

where D is displacement of charge density, ε is the permittivity, and E is the electric field.

To define a system, Hooke's law states that

$$S = sT \tag{1.8}$$

where S is the strain, s is the compliance, and T is the stress.

Equations 1.7 and 1.8 can be combined to form relations,

$$\begin{aligned} S &= [s^E]T + [d]E \\ D &= [d^t]T + [\varepsilon^t]E \end{aligned} \tag{1.9}$$

where $[d]$ is direct piezoelectric effect matrix and $[d^t]$ is converse piezoelectric effect matrix, E denotes zero or constant electric field is found in the system, T indicates zero or constant stress field across the system, and t determines the transposition matrix.

The constitutive equation that represents the direct piezoelectric effect is given by [46]

$$D = dT + \varepsilon E \tag{1.10}$$

where D is electric polarization, d is piezoelectric coefficient matrix, T is the stress vector, ε is the electrical permittivity, and E is the electric field vector.

1.3.3 Piezomagnetic effect

The first observation of piezomagnetic effect was made experimentally in 1960, in the flourides of cobalt and manganese [47]. Piezomagnetic material changes its magnetic properties when put under mechanical strain or deformations in the material by application of magnetic field. Piezomagnetic effect is mainly characterized by coupling between magnetization and mechanical strain of the material.

1.4 Overview of the Thesis

This thesis revolves around first-principles theoretical calculations and analysis of van der Waals heterostructure created using graphene and monolayer ferromagnetic 1T-$CrTe_2$. In Chapter 2, we present an overview of computational methods and formalism used in calculations. For determination of ground state properties, the usage of density functional theory (DFT) is discussed. In Chapter 3, we study electronic and magnetic properties of vdW heterostructure Graphene/1T-$CrTe_2$. As a consequence of external perturbations such as application of perpendicular external electric field, carrier doping, and application of strain, there are changes in the electronic and magnetic properties of Graphene/1T-$CrTe_2$ vdW heterostructure.

Bibliography

[1] R. M. Martin, *Electronic structure: basic theory and practical methods*. Cambridge university press, 2020.

[2] J. Kohanoff, *Electronic structure calculations for solids and molecules: theory and computational methods*. Cambridge university press, 2006.

[3] A. C. Neto, F. Guinea, N. M. Peres, K. S. Novoselov, and A. K. Geim, "The electronic properties of graphene," *Reviews of modern physics*, vol. 81, no. 1, p. 109, 2009.

[4] P. Joensen, R. Frindt, and S. R. Morrison, "Single-layer mos2," *Materials research bulletin*, vol. 21, no. 4, pp. 457–461, 1986.

[5] A. Nagashima, N. Tejima, Y. Gamou, T. Kawai, and C. Oshima, "Electronic dispersion relations of monolayer hexagonal boron nitride formed on the ni (111) surface," *Physical Review B*, vol. 51, no. 7, p. 4606, 1995.

[6] L. D. Landau and E. M. Lifshitz, *Statistical Physics: Volume 5*, vol. 5. Elsevier, 2013.

[7] N. D. Mermin, "Crystalline order in two dimensions," *Physical Review*, vol. 176, no. 1, p. 250, 1968.

[8] J. Venables and G. Spiller, "Nucleation and growth of thin films," in *Surface Mobilities on Solid Materials*, pp. 341–404, Springer, 1983.

[9] B. Feng, J. Zhang, Q. Zhong, W. Li, S. Li, H. Li, P. Cheng, S. Meng, L. Chen, and K. Wu, "Experimental realization of two-dimensional boron sheets," *Nature chemistry*, vol. 8, no. 6, pp. 563–568, 2016.

[10] H. Liu, A. T. Neal, Z. Zhu, Z. Luo, X. Xu, D. Tománek, and P. D. Ye, "Phosphorene: an unexplored 2d semiconductor with a high hole mobility," *ACS nano*, vol. 8, no. 4, pp. 4033–4041, 2014.

[11] M. Dávila, L. Xian, S. Cahangirov, A. Rubio, and G. Le Lay, "Germanene: a novel two-dimensional germanium allotrope akin to graphene and silicene," *New Journal of Physics*, vol. 16, no. 9, p. 095002, 2014.

[12] F.-f. Zhu, W.-j. Chen, Y. Xu, C.-l. Gao, D.-d. Guan, C.-h. Liu, D. Qian, S.-C. Zhang, and J.-f. Jia, "Epitaxial growth of two-dimensional stanene," *Nature materials*, vol. 14, no. 10, pp. 1020–1025, 2015.

[13] J. Ji, X. Song, J. Liu, Z. Yan, C. Huo, S. Zhang, M. Su, L. Liao, W. Wang, Z. Ni, *et al.*, "Two-dimensional antimonene single crystals grown by van der waals epitaxy," *Nature communications*, vol. 7, no. 1, pp. 1–9, 2016.

[14] B. Radisavljevic, A. Radenovic, J. Brivio, V. Giacometti, and A. Kis, "Single-layer mos2 transistors," *Nature nanotechnology*, vol. 6, no. 3, pp. 147–150, 2011.

[15] K. Watanabe, T. Taniguchi, and H. Kanda, "Direct-bandgap properties and evidence for ultraviolet lasing of hexagonal boron nitride single crystal," *Nature materials*, vol. 3, no. 6, pp. 404–409, 2004.

[16] Q. Ji, C. Li, J. Wang, J. Niu, Y. Gong, Z. Zhang, Q. Fang, Y. Zhang, J. Shi, L. Liao, *et al.*, "Metallic vanadium disulfide nanosheets as a platform material for multifunctional electrode applications," *Nano Letters*, vol. 17, no. 8, pp. 4908–4916, 2017.

[17] J. Wang, Y. Xu, and S.-C. Zhang, "Two-dimensional time-reversal-invariant topological superconductivity in a doped quantum spin-hall insulator," *Physical Review B*, vol. 90, no. 5, p. 054503, 2014.

[18] S. Z. Butler, S. M. Hollen, L. Cao, Y. Cui, J. A. Gupta, H. R. Gutiérrez, T. F. Heinz, S. S. Hong, J. Huang, A. F. Ismach, *et al.*, "Progress, challenges, and opportunities in two-dimensional materials beyond graphene," *ACS nano*, vol. 7, no. 4, pp. 2898–2926, 2013.

[19] J. A. Wilson and A. Yoffe, "The transition metal dichalcogenides discussion and interpretation of the observed optical, electrical and structural properties," *Advances in Physics*, vol. 18, no. 73, pp. 193–335, 1969.

[20] C. R. Dean, A. F. Young, I. Meric, C. Lee, L. Wang, S. Sorgenfrei, K. Watanabe, T. Taniguchi, P. Kim, K. L. Shepard, *et al.*, "Boron nitride substrates for high-quality graphene electronics," *Nature nanotechnology*, vol. 5, no. 10, pp. 722–726, 2010.

[21] M. Osada and T. Sasaki, "Two-dimensional dielectric nanosheets: novel nanoelectronics from nanocrystal building blocks," *Advanced Materials*, vol. 24, no. 2, pp. 210–228, 2012.

[22] A. Eftekhari, "Tungsten dichalcogenides (ws 2, wse 2, and wte 2): materials chemistry and applications," *Journal of Materials Chemistry A*, vol. 5, no. 35, pp. 18299–18325, 2017.

[23] A. B. Kaul, "Two-dimensional layered materials: Structure, properties, and prospects for device applications," *Journal of Materials Research*, vol. 29, no. 3, pp. 348–361, 2014.

[24] M. Gibertini, M. Koperski, A. F. Morpurgo, and K. S. Novoselov, "Magnetic 2d materials and heterostructures," *Nature nanotechnology*, vol. 14, no. 5, pp. 408–419, 2019.

[25] R. Peierls, "On ising's model of ferromagnetism," in *Mathematical Proceedings of the Cambridge Philosophical Society*, vol. 32, pp. 477–481, Cambridge University Press, 1936.

[26] J.-U. Lee, S. Lee, J. H. Ryoo, S. Kang, T. Y. Kim, P. Kim, C.-H. Park, J.-G. Park, and H. Cheong, "Ising-type magnetic ordering in atomically thin feps3," *Nano letters*, vol. 16, no. 12, pp. 7433–7438, 2016.

[27] M.-W. Lin, H. L. Zhuang, J. Yan, T. Z. Ward, A. A. Puretzky, C. M. Rouleau, Z. Gai, L. Liang, V. Meunier, B. G. Sumpter, *et al.*, "Ultrathin nanosheets of crsite 3: a semiconducting two-dimensional ferromagnetic material," *Journal of Materials Chemistry C*, vol. 4, no. 2, pp. 315–322, 2016.

[28] B. Huang, G. Clark, E. Navarro-Moratalla, D. R. Klein, R. Cheng, K. L. Seyler, D. Zhong, E. Schmidgall, M. A. McGuire, D. H. Cobden, *et al.*, "Layer-dependent ferromagnetism in a van der waals crystal down to the monolayer limit," *Nature*, vol. 546, no. 7657, pp. 270–273, 2017.

[29] C. Gong, L. Li, Z. Li, H. Ji, A. Stern, Y. Xia, T. Cao, W. Bao, C. Wang, Y. Wang, *et al.*, "Discovery of intrinsic ferromagnetism in two-dimensional van der waals crystals," *Nature*, vol. 546, no. 7657, pp. 265–269, 2017.

[30] M. Bonilla, S. Kolekar, Y. Ma, H. C. Diaz, V. Kalappattil, R. Das, T. Eggers, H. R. Gutierrez, M.-H. Phan, and M. Batzill, "Strong room-temperature ferromagnetism in vse2 monolayers on van der waals substrates," *Nature nanotechnology*, vol. 13, no. 4, pp. 289–293, 2018.

[31] Z. Fei, B. Huang, P. Malinowski, W. Wang, T. Song, J. Sanchez, W. Yao, D. Xiao, X. Zhu, A. F. May, *et al.*, "Two-dimensional itinerant ferromagnetism in atomically thin fe3gete2," *Nature materials*, vol. 17, no. 9, pp. 778–782, 2018.

[32] D. J. O'Hara, T. Zhu, A. H. Trout, A. S. Ahmed, Y. K. Luo, C. H. Lee, M. R. Brenner, S. Rajan, J. A. Gupta, D. W. McComb, *et al.*, "Room temperature intrinsic ferromagnetism in epitaxial manganese selenide films in the monolayer limit," *Nano letters*, vol. 18, no. 5, pp. 3125–3131, 2018.

[33] A. K. Geim and I. V. Grigorieva, "Van der waals heterostructures," *Nature*, vol. 499, no. 7459, pp. 419–425, 2013.

[34] C. Dean, A. Young, L. Wang, I. Meric, G.-H. Lee, K. Watanabe, T. Taniguchi, K. Shepard, P. Kim, and J. Hone, "Graphene based heterostructures," *Solid State Communications*, vol. 152, no. 15, pp. 1275–1282, 2012.

[35] Y. Liu, N. O. Weiss, X. Duan, H.-C. Cheng, Y. Huang, and X. Duan, "Van der waals heterostructures and devices," *Nature Reviews Materials*, vol. 1, no. 9, pp. 1–17, 2016.

[36] D. Zhong, K. L. Seyler, X. Linpeng, N. P. Wilson, T. Taniguchi, K. Watanabe, M. A. McGuire, K.-M. C. Fu, D. Xiao, W. Yao, *et al.*, "Layer-resolved magnetic proximity effect in van der waals heterostructures," *Nature Nanotechnology*, vol. 15, no. 3, pp. 187–191, 2020.

[37] D. Zhong, K. L. Seyler, X. Linpeng, R. Cheng, N. Sivadas, B. Huang, E. Schmidgall, T. Taniguchi, K. Watanabe, M. A. McGuire, *et al.*, "Van der waals engineering of ferromagnetic semiconductor heterostructures for spin and valleytronics," *Science advances*, vol. 3, no. 5, p. e1603113, 2017.

[38] B. Huang, M. A. McGuire, A. F. May, D. Xiao, P. Jarillo-Herrero, and X. Xu, "Emergent phenomena and proximity effects in two-dimensional magnets and heterostructures," *Nature Materials*, vol. 19, no. 12, pp. 1276–1289, 2020.

[39] W. C. Röntgen, "Ueber die durch bewegung eines im homogenen electrischen felde befindlichen dielectricums hervorgerufene electrodynamische kraft," *Annalen der Physik*, vol. 271, no. 10, pp. 264–270, 1888.

[40] I. E. Dzyaloshinskii, "On the magneto-electrical effects in antiferromagnets," *Soviet Physics JETP*, vol. 10, pp. 628–629, 1960.

[41] N. A. Spaldin and M. Fiebig, "The renaissance of magnetoelectric multiferroics," *Science*, vol. 309, no. 5733, pp. 391–392, 2005.

[42] M. Fiebig, "Revival of the magnetoelectric effect," *Journal of physics D: applied physics*, vol. 38, no. 8, p. R123, 2005.

[43] J. Curie and P. Curie, "Développement par compression de l'électricité polaire dans les cristaux hémièdres à faces inclinées," *Bulletin de minéralogie*, vol. 3, no. 4, pp. 90–93, 1880.

[44] G. Lippmann, "Principe de la conservation de l'électricité, ou second principe de la théorie des phénomènes électriques," *Journal de Physique Théorique et Appliquée*, vol. 10, no. 1, pp. 381–394, 1881.

[45] J. Briscoe and S. Dunn, "Piezoelectricity and ferroelectricity," in *Nanostructured Piezoelectric Energy Harvesters*, pp. 3–17, Springer, 2014.

[46] I. Chopra, "Review of state of art of smart structures and integrated systems," *AIAA journal*, vol. 40, no. 11, pp. 2145–2187, 2002.

[47] A. BOROVIK—ROMANOV, "Piezomagnetism in the antiferromagnetic fl uorides of cobalt and manga mse," *Soviet physics JETP*, vol. 11, no. 4, 1960.

Chapter 2

Methods and Formalism

In this chapter, we discuss the theoretical description and the computational methods utilized in our First-principles calculations within the framework of density functional theory. In section 2.1, the many-body electron problem is introduced, and in section 2.2, the concepts of density functional theory (DFT) are discussed, including various approximations and self-consistent methods.

2.1 Introduction

The quantum mechanical Hamiltonian operator $\hat{H}$ of a system made up of interacting electrons and nuclei is given by

$$\hat{H} = -\frac{\hbar^2}{2m_e}\sum_i \nabla_i^2 - \frac{\hbar^2}{2M_I}\sum_I \nabla_I^2 + \frac{e^2}{2}\sum_{i\neq j}\frac{1}{|r_i - r_j|} + \frac{e^2}{2}\sum_{I\neq J}\frac{Z_I Z_J}{|r_I - r_J|}$$

$$-e^2\sum_{i,I}\frac{Z_I e^2}{|r_i - R_I|} \tag{2.1}$$

where $\hbar$ is Planck's constant, m_e and M_I are masses of electron and nuclei, respectively, r_i is the position vector for i^{th} electron, Z_I and R_I are atomic numbers and position vectors of I^{th} ion and e is electronic charge. The first and the second terms represent the kinetic energy

of electrons and nuclei, respectively. The third term constitutes interaction between electrons and fourth term signifies interaction between nuclei. The fifth term is the Coulomb interaction between electron and nuclei, which acts as an external potential (V_{ext}) to the system.

With the Hamiltonian given, the time-independent Schrȯdinger equation can be written as

$$\hat{H}\Psi(\mathbf{R}_I, \mathbf{r}_i) = \epsilon\Psi(\mathbf{R}_I, \mathbf{r}_i) \tag{2.2}$$

where ϵ and $\Psi(\mathbf{R}_I, \mathbf{r}_i)$ are energy eigenvalues and total wavefunction of the system that includes electronic and ionic part.

2.1.1 Born-Oppenheheimer Approximation

The ground state total energy can be obtained from the equation 2.2. Materials have a large number of electrons and ions which are coupled to each other. Since electrons move faster than heavy nuclei, the electrons adiabatically do not undergo any transition between stationary states. This approximation is called adiabatic or Born-Oppenheimer approximation [1] that decouples electronic and nuclear degrees of freedom. After applying approximation to Equation 2.1, it reduces to Hamiltonian

$$\hat{H} = -\frac{\hbar^2}{2m_e}\sum_i \nabla_i^2 + \frac{e^2}{2}\sum_{i\neq j}\frac{1}{|r_i - r_j|} + V_{ext} \tag{2.3}$$

where V_{ext} is the external potential in the background of positive ions.

2.2 Density Functional Theory

Density functional theory is a theory of correlated many-body systems. Density functional theory was developed through the pioneering work of Hohenberg-Kohn in 1964 [2], and Kohn-Sham in 1965 [3], which are described in the following section.

2.2.1 Hohenberg-Kohn Theorem

The Hohenberg-Kohn theorem and Kohn-Sham theorem form the basis for the formulation of density functional theory as an exact theory for the ground state of many-body fermionic systems.

Theorem I: The ground state electron density $n_o(r)$ uniquely determines the external potential except a trivial constant. The ground state properties of a system can be determined when $n_o(r)$ is known.

Theorem II: A universal functional for the energy $E[n]$ can be defined in terms of the density $n_o(r)$, which is valid for any external potential $V_{ext}(r)$. The exact ground state energy is the global minimum of this functional and the density that minimizes the functional is the exact ground state density $n_o(r)$.

The total energy functional, determined by n(r), is given by

$$E_{HK}[n] = T[n] + E_{ee}[n] + \int drV_{ext}(r)n(r) + E_{ion-ion} \tag{2.4}$$

where T[n] and $E_e e$[n] are the kinetic and potential energies of the interacting electron system. These theorems assist in calculating the ground state energy by reducing the minimization problem from 3N to 3 variables. $E_{ion-ion}$ is the Coulomb interaction energy of nuclei.

2.2.2 Kohn-Sham ansatz

In 1965, Kohn and Sham [3] described systems consisting of non-interacting electrons having the same n(r) moving in a mean-field of external potential arising from the electron-electron and electron-ion interactions. The main aim of the Kohn-Sham approach was that if one can find any non-interacting electronic system that produces the same electronic density as that of the interacting system, then the kinetic energy of the electrons can be calculated through one-electron orbitals. According to the Kohn-Sham approach, the energy functional can be

written as

$$\begin{aligned} E_{KS}[n(r)] &= T_s[n(r)] + \frac{1}{2}\int \frac{d^3r d^3r' n(r)n(r')}{|r-r'|} + \int dr V_{ext}(r)n(r) + E_{XC}[n(r)] + E_{ion-ion} \\ &= T_s[n(r)] + E_{Hartree}[n(r)] + \int dr V_{ext}(r)n(r) + E_{XC}[n(r)] + E_{ion-ion} \end{aligned} \tag{2.5}$$

The first term is the kinetic energy of electrons. The second and third terms are the interaction energy between electrons and of electrons with external potential, respectively. The fourth term is the exchange-correlation interaction between electrons.

The Kohn-Sham non-interacting single particle Hamiltonian is

$$H_{KS} = T_s[n] + V_{KS}(r) \tag{2.6}$$

where V_{KS} is Kohn-SHam potential, which is defined as,

$$V_{KS} = V_{ext}(r) + V_{Hartree}(r) + V_{XC}(r) \tag{2.7}$$

where V_{ext}, $V_{Hartree}$, and V_{XC} are external Hartree and exchange-correlation potentials respectively.

Kohn-Sham equations are given as,

$$H_{KS}\Psi_i(r) = \epsilon_i \Psi_i(r) \tag{2.8}$$

The ground state density can be written in terms of Ψ_i(r) as,

$$n(r) = \sum_i |\Psi_i(r)|^2 \tag{2.9}$$

A self-consistent iterative method to solve equations 2.8 is shown in Fig

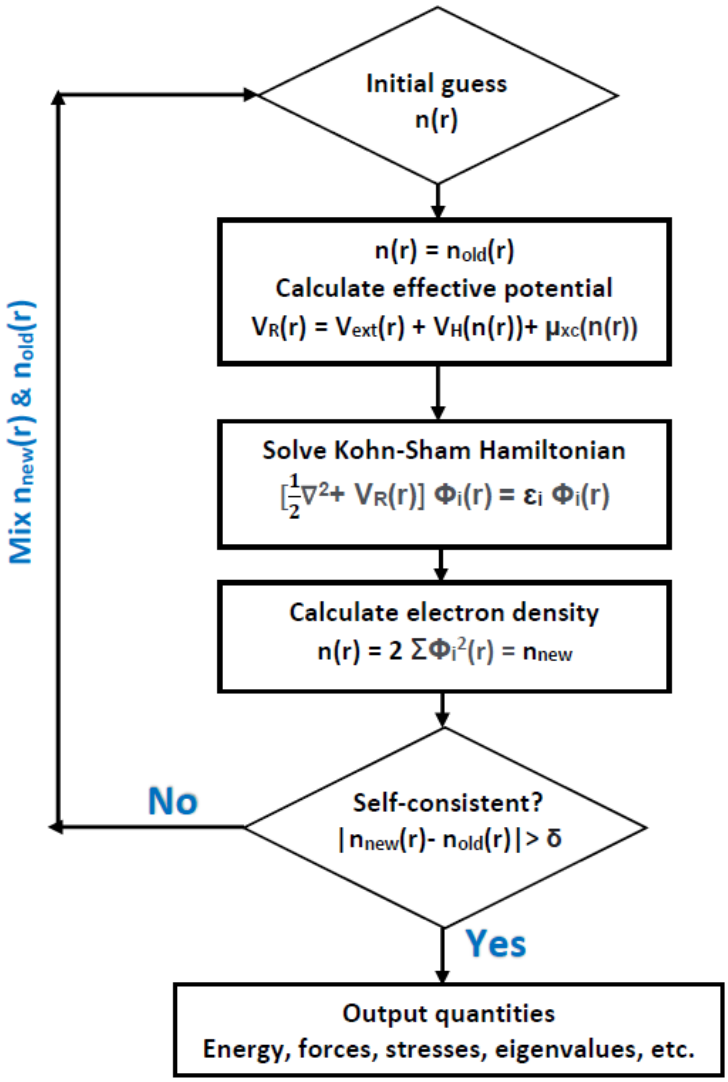

Figure 2.1: Flowchart showing self-consistent iterative solution for Kohn-Sham equations

2.2.3 Exchange-correlation functionals

The exchange-correlation energy E_{XC} is defined as the difference between exact energy and Hartee energy, given as,

$$E_{XC} = T[n] - T_s[n] + E_{ee}[n] - E_{Hartree} \tag{2.10}$$

where T_s[n] and E_{ee}[n] are exact kinetic energy and electron-electron interaction energy, respectively. The exact form of E_{XC} is not known. To determine exchange-correlation energy E_{XC}, two commonly used approximations are local density approximation (LDA) and generalized gradient approximation (GGA).

Local Density Approximation (LDA)

In this approximation, the exchange-correlation energy density at each point is the same as that of a homogeneous electron gas of the same density. In LDA [3], the exchange-correlation energy functional is written as,

$$E_{XC}^{LDA} = \int drn(r)\epsilon_{XC}[n(r)] \tag{2.11}$$

To tackle highly localized orbitals in correlated systems, local density approximation (LDA) is used along with additional orbital dependent term Hubbard U. There are several parameterizations for exchange-correlation. The most commonly used is that of Perdew and Zunger [4].

Generalized Gradient Approximation (GGA)

LDA describes the properties of homogeneous electron gas reasonably well, but it fails when charge density changes very abruptly such as in molecules. In the case of inhomogeneous charge densities, Generalized Gradient Approximation (GGA) [5] is used. In GGA, there are parameterizations such as Perdew andWang (PW91) [6, 7] and Perdew, Burke and Ernzerhof [8]. The exchange-correlation energy can be showed in terms of the gradient and spatial derivatives of the charge density as,

$$E_{XC}^{GGA} = \int drn(r)\epsilon_{XC}(n(r), \Delta n(r)) \tag{2.12}$$

GGA leads to a notable improvement over LDA in estimating energies, bond lengths, and band gap of semiconductors.

2.2.4 Basis sets

A basis set is needed to expand the Kohn-Sham wavefunctions to solve Kohn-Sham equations. The commonly used basis sets are plane waves, atomic orbitals, and mixed basis (a combination of both). The Kohn-sham wavefunction in the plane basis can be expanded as,

$$\Psi_i(r) = \sum_{|G|<G_{cut}} C_{i,(k+G)} e^{i(k+G).r} \tag{2.13}$$

where k is the Bloch wave vector, G is the reciprocal lattice vector and $C_{i,(k+G)}$ is expansion coefficient [9, 10]. The expansion is infinite in principle and a kinetic energy cutoff is used to truncate the set of G vectors and satisfy the condition given below.

$$\frac{\hbar^2}{2m_e}|k+G|^2 \leq E_{cut} \tag{2.14}$$

where E_{cut} is cutoff energy, increased till energy is converged. We have used plane wave basis in all our calculations.

2.2.5 Pseudopotentials

Pseudopotential is another approximation necessary in DFT calculations. The core electrons in solids are tightly bound to the nucleus and are thus not involved in bonding. Valence and semi-core electrons actively participate in chemical bonding and the effective screened potential replaces the interaction of the valence electrons with the nucleus plus the core states. Pseudopotentials are created by considering a cutoff radius (r_c) beyond which the pseudo-wavefunction matches precisely with the true wavefunction (as shown in figure 2.2). The most common forms of pseudopotentials are norm-conserving and ultrasoft. In the region r $<r_c$, if the charge of each pseudo wavefunction is equal to the charge of the all-electron wavefunction, then the pseudopotential is known as norm-conserving pseudopotential [11]. Ultrasoft pseudopotential includes an augmented charge inside the core region to conserve the total charge while making

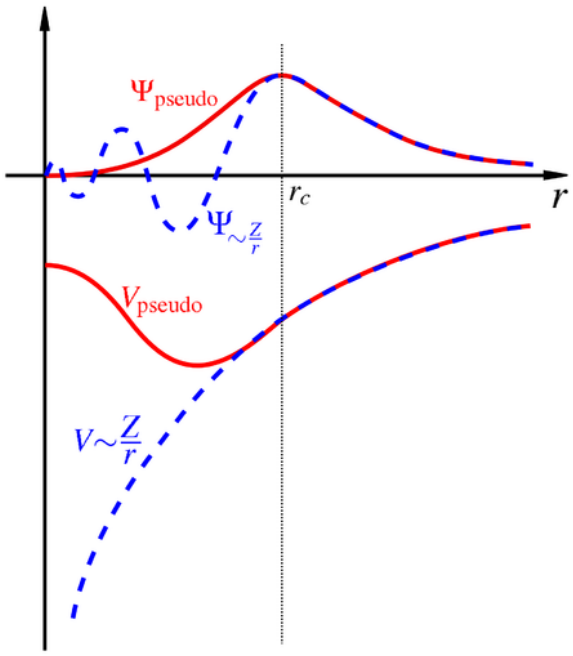

Figure 2.2: Schematic representation of pseudopotential (solid line) and all-electron potential (dotted line) and their corresponding wavefunctions. The figure is taken from https://en.wikipedia.org/wiki/Pseudopotentials

the potential smoother [12]. Over norm-conserving pseudopotentials, ultrasoft pseudopotentials offer computational efficiency and accuracy while maintaining transferability.

2.2.6 Dispersion corrections

GGA functionals cannot describe long-range electron correlations responsible for van der Waals (vdW) forces. Several methods have been developed in recent years to include these dispersive interactions in DFT calculations. There are two classes of dispersion interactions discussed here: (1) semi-empirical corrections to existing local functionals, and (2) the application of non-local exchange-correlation energy functionals to include the London interactions. The inclusion of the DFT-D2 scheme of Grimme [13] in our calculations gives a reasonably accurate treatment of London dispersion interactions. The total energy with dispersion correction is given as,

$$E_{DFT-D2} = E_{KS-DFT} + E_{Disp} \tag{2.15}$$

where E_{KS-DFT} is the self-consistent Kohn-Sham energy. E_{Disp} is the empirical dispersion correction expressed as,

$$E_{Disp} = -S_6 \sum_{i=1}^{N_a-1} \sum_{j=i+1}^{N_a} \frac{C_6^{ij}}{R_{ij}^6} f_{dmp}(R_{ij}) \tag{2.16}$$

where N_a refers to number of atoms in the system, S_6 is the global scaling factor that depends on functional and R_{ij} is the interatomic distance. C_6^{ij} denotes the dispersion coefficient for atom pain i and j expressed as,

$$C_6^{ij} = \sqrt{C_6^i C_6^j} \tag{2.17}$$

A damping function is used to avoid near-singularities at a smaller value of R in equation 2.16, which is given as,

$$F_{Damping}(R_{ij}) = \frac{1}{1 + e^{-d(\frac{R_{ij}}{R_r - 1})}} \tag{2.18}$$

where d is the dispersion correction parameter to the total energy and is fixed to value of 20 by Grimme to give accurate dispersion energies, and R_r denotes the sum of atomic van der Waals radii.

2.2.7 Electron-electron correlations

DFT fails to deal adequately with electron-electron correlations, which are treated averagely. Although such a prescription is highly successful in most cases, it fails when the electron-electron correlation becomes strong as d and f orbitals are present in the systems. The Hubbard model is a model of interacting particles in a lattice with two terms in Hamiltonian. The first is a kinetic term that allows the hopping of particles between sites of the lattice, and the second is the potential term that consists of an on-site interaction. The inclusion of the Hubbard term in DFT simulations improves the prediction of electron localization, preventing the incorrect prediction of metallic conduction in insulating systems. The LDA+U method [14] consists of a correction to the LDA (or GGA) energy functional to better describe electronic correlations [15]. The Hubbard model behaves differently from a tight-binding model when electrons interact

strongly. For example, the Hubbard model predicts the existence of Mott insulators correctly. A Hubbard model can also be studied using the dynamical mean-field theory (DMFT). In addition, the U correction can enhance the description of physical properties other than the electronic structure, including magnetic and structural properties of correlated systems. By simply adding a semiempirically tuned numerical parameter U to the DFT+U method, it can account for the underestimated electronic interactions [16].

Bibliography

[1] Max Born and Robert Oppenheimer. Zur quantentheorie der molekeln. *Annalen der physik*, 389(20):457–484, 1927.

[2] Pierre Hohenberg and Walter Kohn. Inhomogeneous electron gas. *Physical review*, 136(3B):B864, 1964.

[3] Walter Kohn and Lu Jeu Sham. Self-consistent equations including exchange and correlation effects. *Physical review*, 140(4A):A1133, 1965.

[4] JP Perdew, ER McMullen, and Alex Zunger. Density-functional theory of the correlation energy in atoms and ions: a simple analytic model and a challenge. *Physical Review A*, 23(6):2785, 1981.

[5] Richard M Martin. *Electronic structure: basic theory and practical methods*. Cambridge university press, 2020.

[6] John P Perdew, P Ziesche, and H Eschrig. Electronic structure of solids' 91, 1991.

[7] John P Perdew, John A Chevary, Sy H Vosko, Koblar A Jackson, Mark R Pederson, Dig J Singh, and Carlos Fiolhais. Atoms, molecules, solids, and surfaces: Applications of the generalized gradient approximation for exchange and correlation. *Physical review B*, 46(11):6671, 1992.

[8] John P Perdew, Kieron Burke, and Matthias Ernzerhof. Generalized gradient approximation made simple. *Physical review letters*, 77(18):3865, 1996.

[9] Paolo Giannozzi, Stefano Baroni, Nicola Bonini, Matteo Calandra, Roberto Car, Carlo Cavazzoni, Davide Ceresoli, Guido L Chiarotti, Matteo Cococcioni, Ismaila Dabo, et al. Quantum espresso: a modular and open-source software project for quantum simulations of materials. *Journal of physics: Condensed matter*, 21(39):395502, 2009.

[10] Xavier Gonze, J-M Beuken, Razvan Caracas, F Detraux, M Fuchs, G-M Rignanese, Luc Sindic, Matthieu Verstraete, G Zerah, F Jollet, et al. First-principles computation of material properties: the abinit software project. *Computational Materials Science*, 25(3):478–492, 2002.

[11] DR Hamann, M Schlüter, and C Chiang. Norm-conserving pseudopotentials. *Physical Review Letters*, 43(20):1494, 1979.

[12] David Vanderbilt. Soft self-consistent pseudopotentials in a generalized eigenvalue formalism. *Physical review B*, 41(11):7892, 1990.

[13] Stefan Grimme. Semiempirical gga-type density functional constructed with a long-range dispersion correction. *Journal of computational chemistry*, 27(15):1787–1799, 2006.

[14] Matteo Cococcioni. The lda+ u approach: A simple hubbard correction for correlated ground states. *Correlated Electrons: From Models to Materials Modeling and Simulation*, 2:4–4, 2012.

[15] John Hubbard. Electron correlations in narrow energy bands. *Proceedings of the Royal Society of London. Series A. Mathematical and Physical Sciences*, 276(1365):238–257, 1963.

[16] Burak Himmetoglu, Andrea Floris, Stefano De Gironcoli, and Matteo Cococcioni. Hubbard-corrected dft energy functionals: The lda+ u description of correlated systems. *International Journal of Quantum Chemistry*, 114(1):14–49, 2014.

Chapter 3

van der Waals heterostructure of graphene and ferromagnetic 1T-$CrTe_2$ monolayer

3.1 Introduction

Graphene is composed of a single layer of carbon atoms arranged in a 2D honeycomb lattice. Various remarkable properties of graphene have been reported, such as zero band gap, high Young's modulus, excellent thermal and electrical conductivity, and high surface area [1]. The extraordinary properties of graphene make it a promising material for a wide range of applications such as high-speed electronics, energy generation, hybrid materials, sensors, and even DNA sequencing [2]. In the monolayer limit, materials spans a wide range of electronic behaviors, for example, graphene is a semimetal [3], hexagonal boron nitride (hBN) is a wide-gap insulator [4], MoS_2 is a semiconductor [5], $NbSe_2$ is a superconductor [6], CrI_3 is a ferromagnet [7], and WTe_2 is a quantum spin Hall insulator [8]. Modifications of two-dimensional materials, such as metals, semimetals, topological insulators, and semiconductors, have mainly been achieved through doping, adding magnetic impurities, and combining a substrate, where externally introduced

defects were used to modify their properties [9]. The idea of spin injection into graphene by the proximity effect is currently an exciting and developing field of research. Because the graphene layer naturally short-circuits on magnetic conducting substrates, it restricts the design of new types of devices. The discovery of atomic thin crystals with long-range magnetic order has opened up new research opportunities in 2D magnetism and low-power spintronic devices [10].

Two-dimensional vdW materials are of great interest and their true potential lies in the possibility of mixing and matching atomically thin layers of various crystals to form heterostructures [11]. Van der Waals heterostructures formed by two-dimensional materials are emerging as materials of great interest. in 2D crystals, strong covalent bonds provide sufficient in-plane stability and relatively weak vdW interactions to keep the stack together [12]. Magnetic proximity effect studies on vdW heterostructures from various 2D materials have been reported such as graphene and EuS [13], graphene and CrI_3 [14], graphene and hexagonal boron nitride [15], and CrI_3 on WTe_2 [16]. Recently, in graphene/BiFeO3 heterostructures, large spin splitting, as well as tuning of the interfacial exchange coupling, was demonstrated [17]. Various atomic layers have been found to possess magnetic order, including Fe_3GeTe_2 [18], $MnSe_2$ [19] and VSe_2 [20].

The proximity effect is an important tool in manipulating spintronics [9]. Doping, defects, and coupling with magnetic substrates have been used previously to create externally induced magnetic moments in layered atomic crystals. Extrinsic spin injections using robust exchange interactions are challenging, and magnetic substrates coupled with 2D materials inhibit vdW heterostructures that are necessary for developing advanced spintronic devices [21]. Heterostructures have promising applications in nanoelectronics, optoelectronics, and photocatalyst fields. For practical application, vdW heterostructures should have flexible and controllable electronic properties, especially a tunable direct bandgap. External application of electric field and strain are commonly used to modulate the bandgap of 2D heterostructures. By incorporating a magnetic material into non-magnetic material, the time-reversal symmetry is broken and the electronic structure is altered due to hybridization with the magnetic layer.

The motivation behind the present work comes from the successful experimental realization of ferromagnetic vdW 1T-$CrTe_2$ monolayer [22]. 1T-$CrTe_2$ is a layered compound with ferromagnetism critical temperature of 320 K and room temperature for bulk phase and two-dimensional phase, respectively [23]. Recent work on 2D magnetic 1T-$CrTe_2$ has attracted considerable attention for applications in magnetic sensors and storage devices due to its strong magnetic anisotropy and high Curie temperature [24]. $CrTe_2$ is a transition metal dichalcogenide (TMD) that crystallizes in a 1T phase, in which the chromium hexagonal planes are sandwiched by tellurium layers [25]. Here, we have investigated the magnetic proximity effect in the van der Waals heterostructure formed by graphene and monolayer T-$CrTe_2$. Our theoretical calculations indicate that the electric and magnetic properties of Graphene/1T-$CrTe_2$ can be tuned using carrier doping, strain, and external electric field.

3.2 Computational Details

Our first-principles calculations are based on density functional theory (DFT) within a Generalized Gradient Approximation (GGA) [26] of the exchange-correlation energy with a functional parameterized by Perdew-Burke-Ernzerhof (PBE) as implemented in QUANTUM ESPRESSO (QE) package [27], which employs plane wave basis and pseudopotentials. The interactions between ionic cores and valence electrons are represented using Projector Augmented Wave (PAW) scalar relativistic pseudopotentials [28, 29]. We use an energy cutoff of 60 Ry to truncate the plane-wave basis used to represent wave functions and a charge density cutoff of 500 Ry. In calculations for pristine graphene supercell of 3x3, we have taken energy cutoff of 40 Ry and charge density cutoff of 400 Ry. The van der Waals (vdW) interactions are taken into account between graphene and ferromagnetic monolayer 1T-$CrTe_2$ using the DFT-D2 method proposed by Grimme [30]. The occupancy numbers of electronic states are smeared using the Fermi–Dirac distribution and a smearing width (k_BT) of 0.003 Ry. The correlation effects for Cr-3d orbitals are considered by including the DFT+U approach suggested by Anisimov et

al. [31] and Liechtenstein et al. [32] with Hubbard U parameter of 2 eV [33] as used by S. Li et al. All calculations on heterostructure and monolayer 1T-$CrTe_2$ are performed by taking ferromagnetic ordering at Cr atoms. We imposed a vacuum of 8 Å in z-direction all calculations. A 3 x 3 x 1 supercell of graphene is used to lattice match with 2 x 2 x 1 supercell of 1T-$CrTe_2$ with a lattice mismatch of around 0.54 %. C atoms of graphene and Cr and Te atoms of $CrTe_2$ are all relaxed to obtain the heterostructure. The total energy has been calculated using an accuracy of $10^{-}8$ Ry using the Davidson method of diagonalization with overlap matrix. Brillouin zone integrations were made on a Monkhorst-Pack grid of 7 x 7 x 1 k-points [34] for heterostructure and 12 x 12 x 1 for 3 x 3 supercell of pristine graphene. The convergence threshold values on the total energy and force were 10^{-6} Ry and 10^{-5} Ry/a.u., respectively. The external electric field is applied in the direction perpendicular to the plane of the Graphene/1T-$CrTe_2$. A biaxial in-plane strain ranging from -1.5% to 1.5% is applied along x and y-directions.

3.3 Results and Discussion

3.3.1 Model Structure

1T-$CrTe_2$ has a layered structure belonging to space group P$\bar{3}$m1 (No. 164). The primitive unit cell consists of 18 carbon, 4 chromium, and 8 tellurium atoms. Single-layer of graphene is composed of carbon atoms arranged in a honeycomb lattice. To construct heterostructure, we place a 3x3 supercell of graphene on a 2x2 supercell of 1T-$CrTe_2$, having a lattice mismatch of around 0.54 %. Monolayer 1T-$CrTe_2$ has a hexagonal structure just like graphene. The lattice constant of pristine graphene is 2.46 Å, and the C-C bond length is 1.42 Å, consistent with the earlier reported value. Monolayer 1T-$CrTe_2$ has a hexagonal structure. After performing structural relaxation, the optimized lattice constant is 3.71 Å [35]. Due to Octahedron coordination, 3d orbitals of 1T-$CrTe_2$ splits into e_g and t_{2g}. The top and side views of the heterostructure of graphene and monolayer T-$CrTe_2$ are shown in figure 3.1(a). The heterostructure is fully relaxed considering ferromagnetic ordering at chromium atoms. The interlayer distance be-

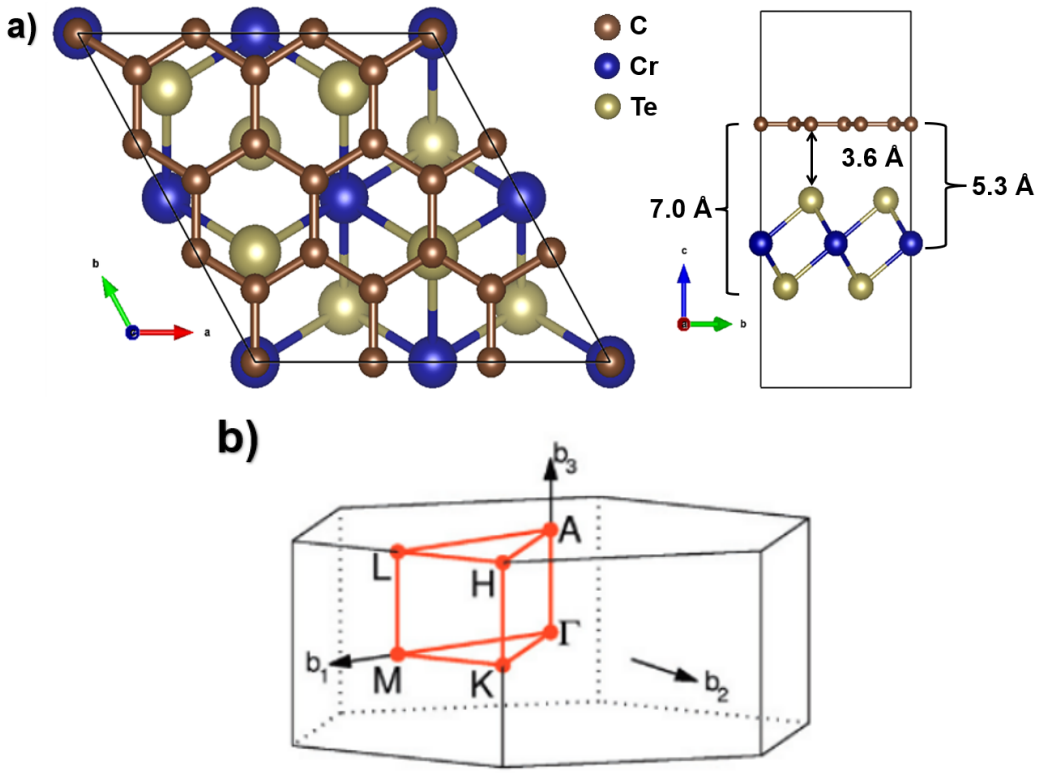

Figure 3.1: (a) Model structure of Graphene/1T-$CrTe_2$ heterostructure. Top and side views of periodic unit cell of Graphene/1T-$CrTe_2$ (AB stacking). Brown, blue and yellow balls represent C, Cr, and Te atoms respectively (b) Brillouin zone of Hexagonal lattice system [36].

Lattice Parameters	**Pristine graphene**	**Monolayer 1T-CrTe**	**Graphene/1T-$CrTe_2$ heterostructure**
a,b (Å)	2.46	3.71	7.64
supercell	3x3	2x2	1x1

Table 3.1: The calculated lattice parameters of monolayers and heterostructure

tween graphene and monolayer $CrTe_2$ (Graphene/1T-$CrTe_2$) is 3.6 Å. Also, figure 3.1(a) shows graphene to chromium and graphene to tellurium interlayer distances. The Brillouin zone of hexagonal lattice is shown in figure 3.1(b). The lattice constant is 7.64 Å. To attain the most stable configuration, the graphene layer is moved along x and y-directions by 0.33 and 0.66 crystal coordinates, and there is a negligible difference in energy. The lattice constants of monolayers and heterostructure are shown in the table below. To characterize the stability of the interface, we calculated the binding energy between graphene and 1T-$CrTe_2$ layers. The

interface binding energy is defined as,

$$E_B = \frac{[E_{Graphene/1T-CrTe_2} - E_{Graphene} - E_{1T-CrTe_2}]}{N} \tag{3.1}$$

where E_b is the binding energy; $E_{graphene/1T-CrTe_2}$, $E_{Graphene}$ and $E_{1T-CrTe_2}$ are the total energy of the vdW heterostructure, pristine graphene layer and monolayer 1T-$CrTe_2$, respectively. N is the number of atoms in the heterostructure. [37]. The binding energy obtained without including vdW correction is 4.8 meV/atom and with the inclusion of vdW correction is -160 meV/atom. The negative binding energy of the heterostructure with vdW interactions indicates that the fabrication of the heterostructure is energetically feasible. Thus, the weak vdW interactions play a non-trivial role in the heterostructure.

3.3.2 Electronic Structure and Projected Density of States

The electronic structure of the supercell of (3x3) graphene is shown in figure 3.2(a). The red and black bands show spin up and spin down respectively. In pristine graphene, spin-up and spin-down bands are degenerate. The K and K' points in the unit cell are folded to Γ point in the (3x3) supercell of graphene. Any wavevector in the higher Brillouin zones can be folded to its corresponding wavevector in the first Brillouin zone via the translational symmetry operation [38]. The pristine graphene shows two pairs of bands in the 3x3 supercell, and since spin-polarized calculations are done, there are eight bands of graphene, including four bands each for the spin up and spin down. The eight bands of graphene around the Γ point appears to be preserved. The spin-polarized electronic structure of graphene/1T-$CrTe_2$ is plotted, as shown in figure 3.2(b) along with the spin-polarized partial density of states. The partial density of states describes the contribution of particular atomic orbitals in the graphene/1T-$CrTe_2$ heterostructure. The states near Fermi level have maximum contribution from C-p, Cr-d and Te-p orbitals. The monolayer of 1T-$CrTe_2$ is metallic and pristine graphene is semimetallic in nature. Graphene/1T-$CrTe_2$ heterostructure shows metallic characteristics.

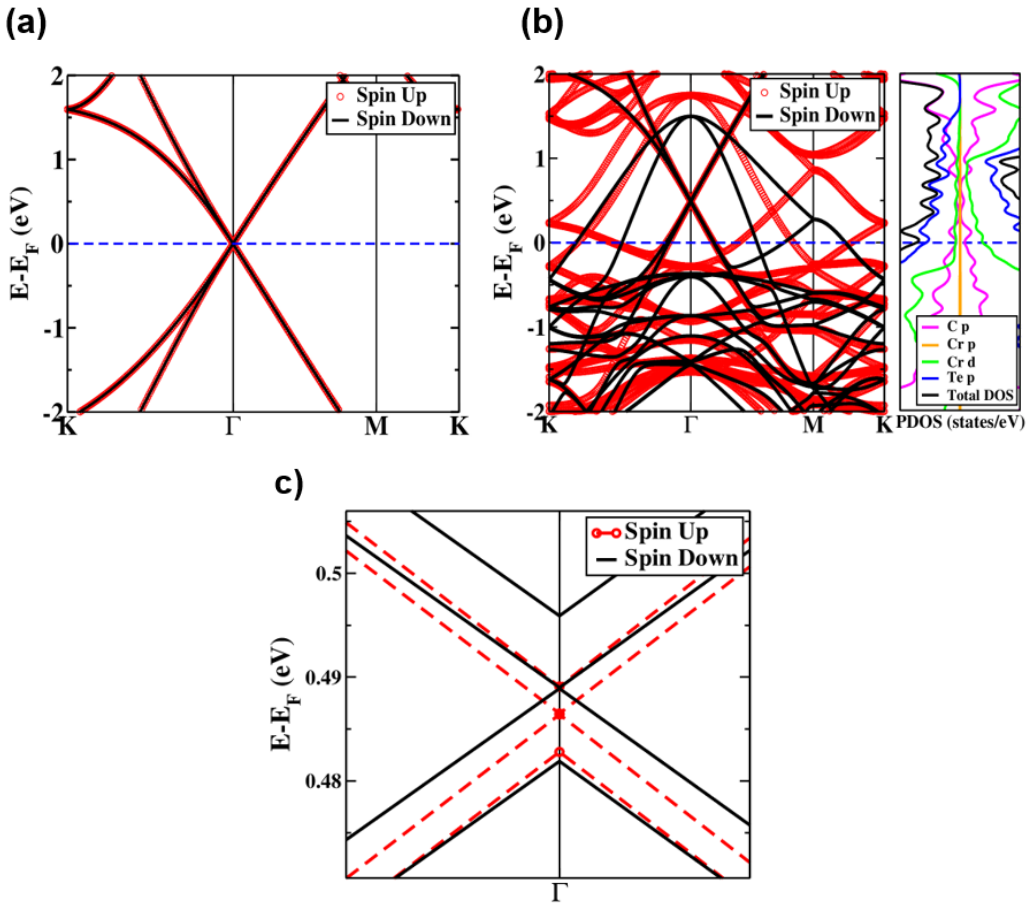

Figure 3.2: Spin-resolved electronic structure of (a) Pristine Graphene of supercell (3x3) (b) heterostructure of Gr/1T-CrTe2 along with the spin-resolved projected density of states (c) Magnified electronic structure of heterostructure near Γ point

The inclusion of 2D magnetic layer below graphene layer shifts and changes the electronic structure of the graphene/1T-$CrTe_2$ heterostructure remarkably due to different chemical and magnetic environment. We note that the bands of 1T-$CrTe_2$ are not affected significantly and the graphene Dirac points are shifted above the Fermi level 0.48 eV and 0.49 eV for spin up and spin down bands. However, the spin up and spin down bands near Γ point reveal a significant change as shown in figure 3.2(c). There are four spin up and four spin down bands. The spin up and spin down Dirac points have energy gap of about 2.5 meV. The band gap arises from the proximity induced exchange splitting of spin up and spin down bands. It is due to the exchange field in graphene induced by the 1T-$CrTe_2$ layer containing ferromagnetic

Cr atoms. The magnetic ordering of heterostructure is ferromagnetic in the ground state having magnetic moment of 10.69 μ_B per cell. Whereas, magnetic moment for monolayer 1T-$CrTe_2$ is 10.64 μ_B per cell with an increase of 20% in comparison to bulk counterpart having magnetic moment of 10.44 μ_B per cell. The increase in the magnetic moment by 3% in heterostructure with respect to the monolayer 1T-$CrTe_2$ indicates magnetic proximity effect [39]. In the heterostructure Graphene/1T-$CrTe_2$, inversion symmetry and time reversal symmetry are broken due to ferromagnetic layer of 1T-$CrTe_2$. In figure 3.2(c), out of the four spin up bands, two bands have been observed to undergo a band splitting of about $\epsilon_1 = 2.6$ meV and $\epsilon_2 = 3.6$ meV. Similarly for spin down, two of the four bands have undergone band splitting of $\epsilon_1 = 6.9$ meV and $\epsilon_2 = 7.0$ meV. In the next section, we will discuss regarding which orbitals of Cr, Te and contribute to the states near Fermi level.

3.3.3 Orbital-resolved Electronic Structure

Orbital resolved electronic structure or fat band structure is used to visualize the contributions of different orbitals to the electronic structure of the system. To get better understanding, we calculate the projection of individual bands onto some orbital (such as s,p,d,f orbitals).In fatbands we show the projections as functions of both momentum and energy i.e, projection onto orbitals with different angular momentum such as l=0,1,2. In order to study the contribution of each atomic orbital of atom to each band in the electronic structure, orbital-resolved electronic structure of Graphene/1T-$CrTe_2$ heterostructure for C, Cr and Te atoms are plotted, see figure 3.3(a)-(h). Spin up and spin down bands at Dirac cone have predominant C-p_z character. As shown in figure 3.3(c), (e) and (g), for spin up bands of heterostructure, the states near Fermi level have contributions from Cr-d_{z^2}, Cr-$d_{x^2-y^2}$, Te-p_x and Te-p_y orbitals. As shown in figure 3.3(d), (f) and (h), the states near Fermi level in spin down bands of heterostructure has contributions from Cr-$d_{x^2-y^2}$, Te-p_x and Te-p_y orbitals.

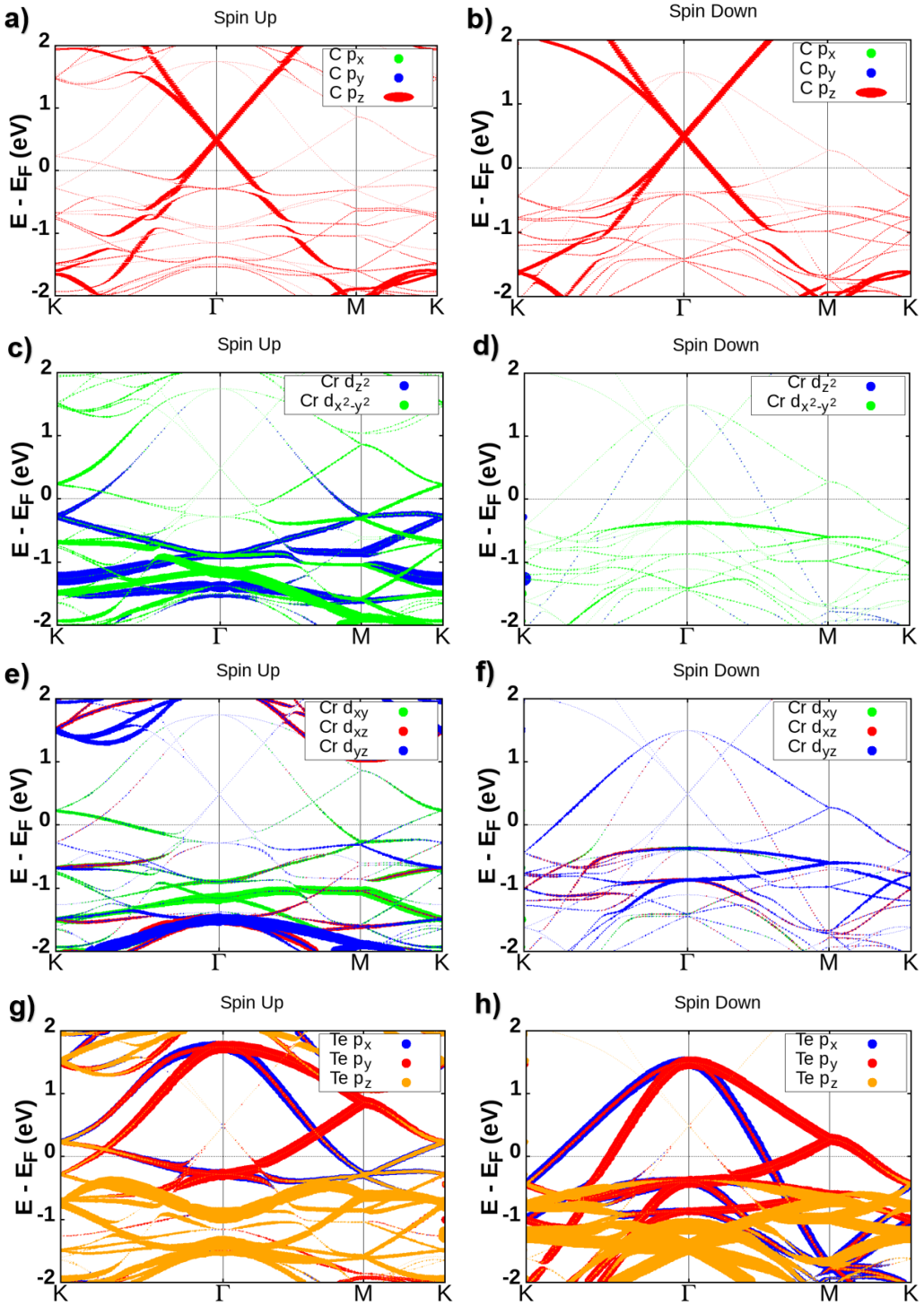

Figure 3.3: Orbital-resolved electronic structure of Graphene/1T-$CrTe_2$ in spin up and spin down channels for [(a) and (b)] C, [(c) - (f)] Cr, [(g) and (h)] Te atoms.

3.3.4 Work Function and Charge Transfer

Work function is defined as the minimum amount of energy required to remove one electron from the highest occupied level to infinity. It is calculated using

$$\phi = E_{vac} - E_F \tag{3.2}$$

where E_{vac} is energy of vacuum and E_F is the Fermi energy. From equation 3.2, we can obtain the ϕ work function for graphene, monolayer 1T-$CrTe_2$ and heterostructure Graphene/1T-$CrTe_2$ as shown in figure 3.4(a)

Materials	**Work Function (eV)**
Pristine graphene	4.26
Monolayer 1T-$CrTe_2$	5.35
Undoped graphene/1T-$CrTe_2$ heterostructure	5.07
Doped[1] graphene/1T-$CrTe_2$ heterostructure	4.68

Table 3.2: Work functions of monolayers and heterostructure calculated from macroscopic average potential plots

The shift of the Dirac point above Fermi level can be accounted by charge transfer. To illustrate the charge transfer, we calculated the electron density difference, which is obtained by subtracting the charge densities of the isolated graphene and 1T-$CrTe_2$ slabs from the total charge density in the heterostructure. The electron density difference of the heterostructure Graphene/1T-$CrTe_2$ can be obtained using,

$$\Delta\rho = \Delta\rho_{Hetero} - \Delta\rho_{Gr} - \Delta\rho_{1T-CrTe_2} \tag{3.3}$$

where $\Delta\ \rho_{Hetero}$, $\Delta\ \rho_{Gr}$ and $\Delta\ \rho_{1T-CrTe_2}$ are charge densities of heterostructure, graphene and

[1]doping heterostructure with one electron per two unit cells

1T-$CrTe_2$ respectively. Figure 3.4(b) shows the charge density difference of the heterostructure.

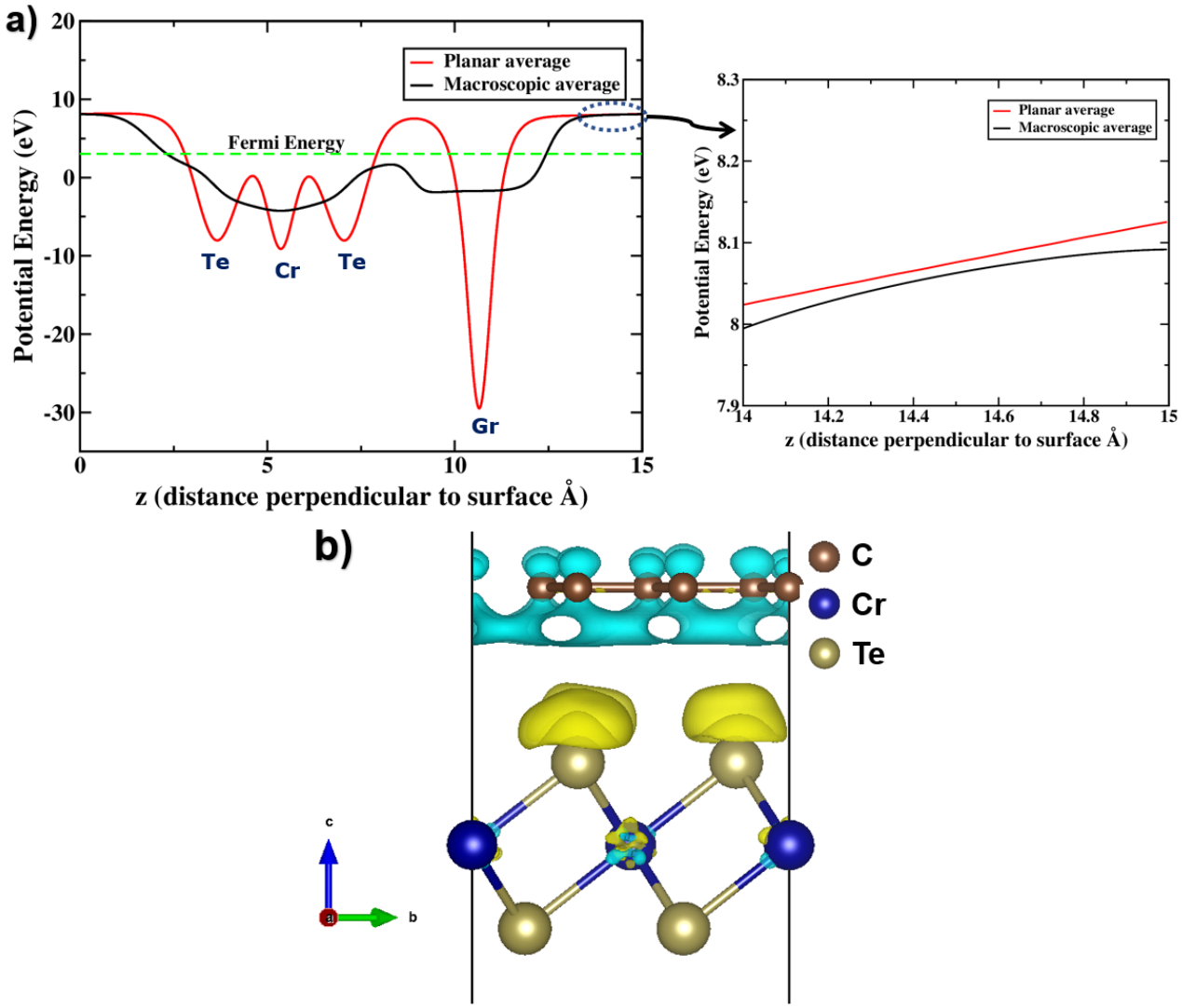

Figure 3.4: (a)The macroscopic average and the average of the electrostatic potential for undoped heterostructure of Graphene/1T-$CrTe_2$ (b) Charge density difference with the isosurface value of 0.00022 e/Å^3. Cyan and yellow colors represent electron depletion and accumulation respectively.

The yellow and cyan represents electron accumulation and depletion respectively. Thus, the electron transfers from graphene layer to monolayer 1T-$CrTe_2$ layer. When two layers with different work functions come in contact with each other, the charges redistribution to equalize the E_F between the layers. This charge redistribution results in intrinsic dipole moment and the polarization is 0.12 $\mu C/cm^2$. This refers to p-type doping of the graphene layer, which

results from electron transfer from graphene to the 1T-$CrTe_2$ layer. In the next section, we will disuss magnetic properties of heterostructure.

3.3.5 Magnetic Properties

In the bulk and two-dimensional phase, 1T-$CrTe_2$ has a ferromagnetism critical temperature of 320 K and room temperature, respectively [23]. The spin density plots are shown in figure 3.5(a) and 3.5(b), which clearly shows that the Cr atoms contribute most to the magnetic moment of the heterostructure (3.11 μ_B), whereas each Te atom provides -0.233 μ_B to the magnetic moment. The ferromagnetic properties of the heterostructure come from Cr atoms. The magnetic ordering of heterostructure is ferromagnetic in the ground state having magnetization of 10.69 μ_B per cell.

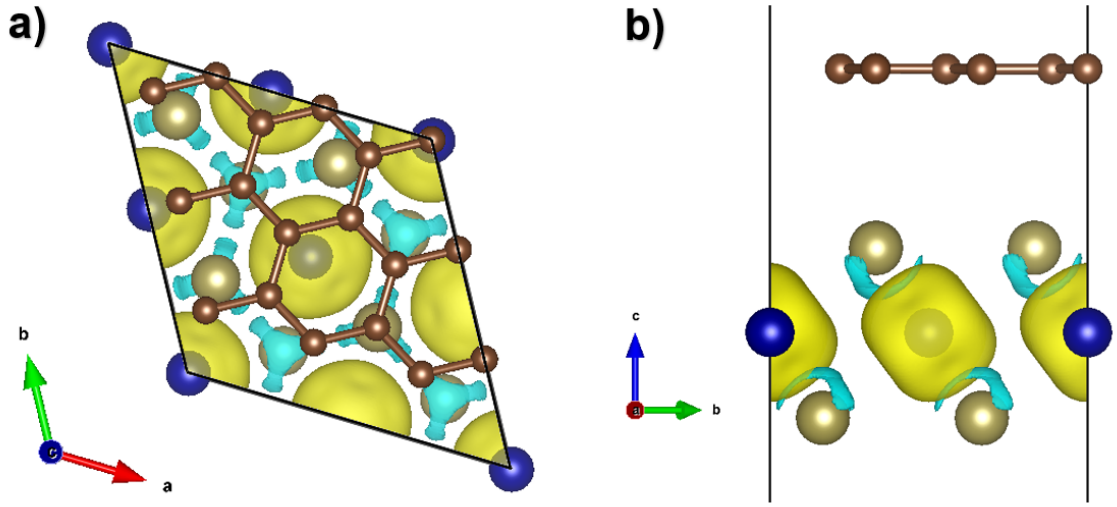

Figure 3.5: (a) Top and (b) side views of the heterostructure showing spin density distribution, with yellow and cyan colors showing positive and negative magnetization density on Cr and Te atoms respectively.

3.3.6 Carrier doping

One electron per two unit cells is doped in the graphene/1T-$CrTe_2$ vdW heterostructure. Figure 3.6(a) shows a schematic of gap opening at Dirac point of the heterostructure due to magnetic

proximity effect and doping for spin up bands. The spin-polarized electronic structure of one electron doped per two unit cells of Graphene/1T-$CrTe_2$ heterostructure is plotted in figure 3.6(b).

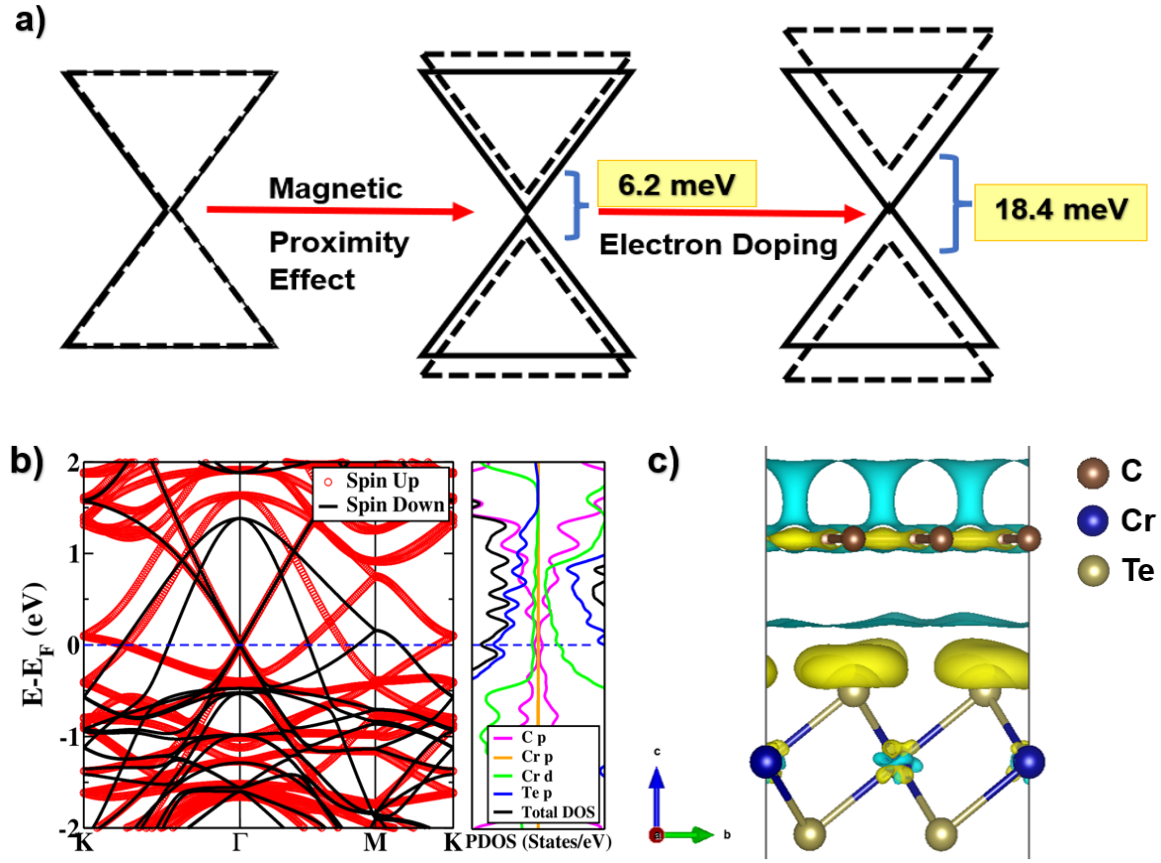

Figure 3.6: (a) Schematic diagram of gap opening in Graphene and 1T-$CrTe_2$ vdW heterostructure for spin up channel (b) Spin-resolved electronic structure of Graphene/1T-$CrTe_2$ after one electron per two unit cells doped along with the spin-resolved projected density of states (PDOS) (c) Charge density difference with the isosurface value of 0.0001 e/Å^3 of one electron per two unit cells doped Graphene/1T-$CrTe_2$ vdW heterostructure. Cyan and yellow colors represent electron depletion and accumulation respectively.

Due to the n-type doping of heterostructure, the band gap open at Γ point are $\epsilon_1 = 8.5$ meV and $\epsilon_2 = 9.9$ meV, which are comparatively higher than the undoped heterostructure. It should be noted that the Dirac cone of graphene at Γ point has shifted to the Fermi level and shows enhanced electron transfer from Graphene to 1T-$CrTe_2$ layer, as shown in figure 3.6(c). To realize change in dipole moment after electron doping, the planar and macroscopic average

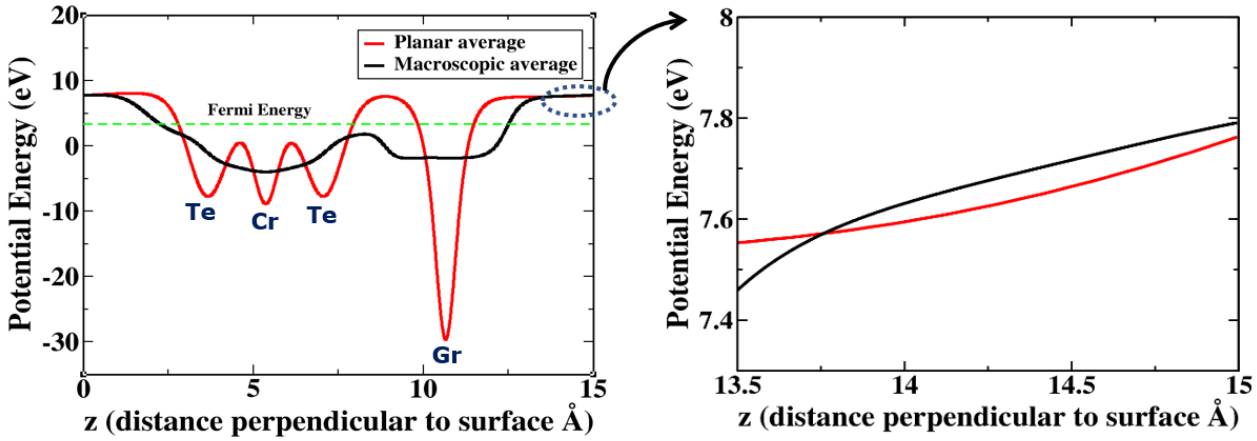

Figure 3.7: The macroscopic average and the average of the electrostatic potential for one electron doped per two unit cells in heterostructure of Graphene/1T-$CrTe_2$

potentials are shown in figure 3.7. The strengthened charge distribution results in the change in induced dipole moment which results in a polarization of around 0.16 $\mu C/cm^2$.

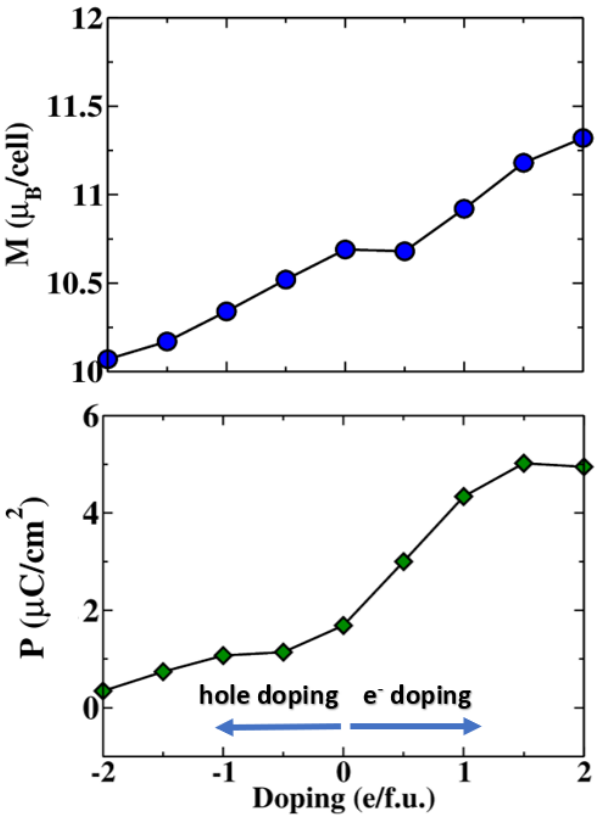

Figure 3.8: Magnetization M and polarization P as a function of hole and electron doping in Graphene/1T-$CrTe_2$ vdW heterostructure

Carrier doping can play a significant role in material properties. In figure 3.8, we have shown the variation of magnetization and polarization with respect to hole and electron doping. As a result of electron or hole doping, magnetization per cell varies linearly. On the other hand, polarization decreases modestly with hole doping and varies drastically with electron doping. This shows that there is possible magnetoelectric coupling in the heterostructure, which is discussed in subsequent section.

3.3.7 External Electric Field

In addition to doping, a perpendicular external electric field may be used to tune the electronic and magnetic properties of vdW heterostructures. Figure 3.9(a) depicts the change in magnetization with change in polarization for relaxed and self-consistent calculations, which implies significant magnetoelectric coupling. Dzyaloshinskii [40] was the first to show a violation of time-reversal symmetry explicitly for a particular system (antiferromagnetic Cr_2O_3), which was soon followed by experimental confirmation of electric-field-induced magnetization. The linear magnetoelectric effect was studied by Dzyaloshinskii from a symmetry point of view [41]. A perpendicular external electric field is applied in z-directions ranging from -0.5 V/Åto 0.5

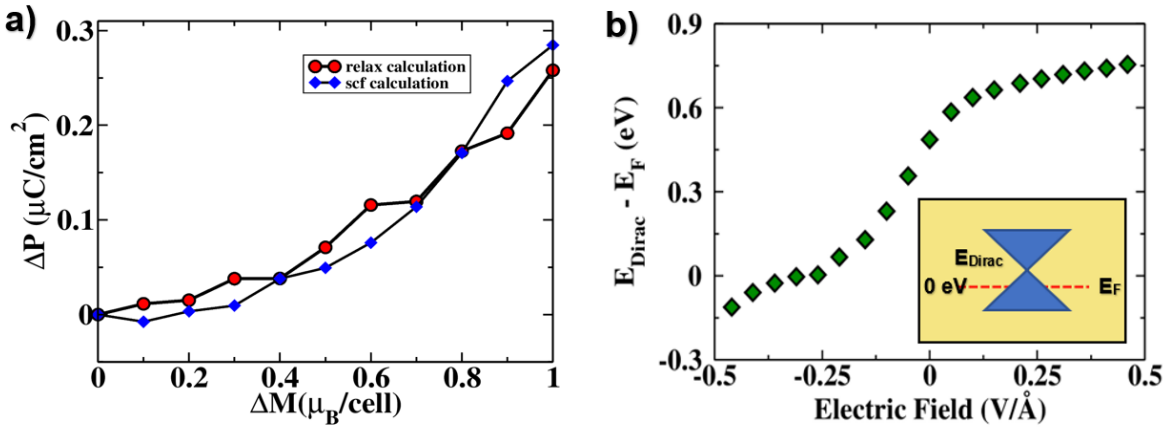

Figure 3.9: (a) Change in polarization with change in magnetization considering self-consistent and relaxation of structure (b) The Fermi level shift under external electric field in the z-direction

V/Å. Figure 3.9(b) shows that the Fermi level is shifts deeper towards the valence band and

into conduction band for electric field along positive and negative z-direction, respectively. In other words, the Dirac points shift to higher energy and lower energy with respect to the Fermi level for positive and negative electric field, respectively.

The change in electronic structure with externally applied electric field can be quantified in terms of charge density difference profile. In undoped heterostructure, the electron transfer from graphene to 1T-$CrTe_2$ layer creates an intrinsic electric field across the heterostructure and by providing a positive external field in the z-direction, additional electrons are transferred from Graphene to the 1T-$CrTe_2$ layer, which strengthens the p-type behaviour. For negative electric field applied in z-direction, the electron transfer shows n-type behavior.

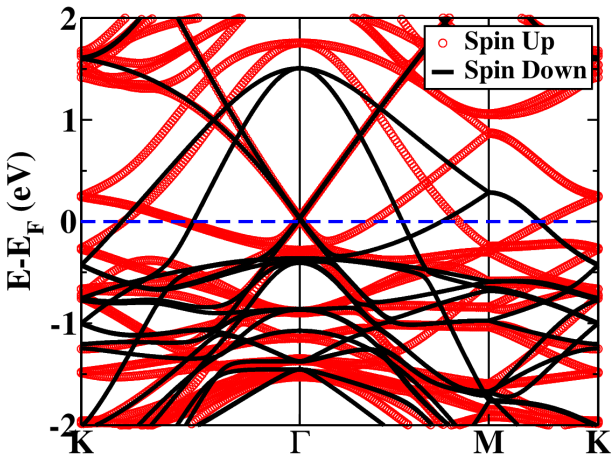

Figure 3.10: Spin-resolved electronic structure of Graphene/1T-$CrTe_2$ under negative electric field strength of 0.26 V/Å

At a particular value of negative electric field strength of 0.26 V/Å, the Dirac points of graphene pin at the Fermi level as shown by spin-resolved electronic structure of Graphene/1T-$CrTe_2$ in figure 3.10. It is observed that the metallic behavior of heterostructure remains intact. The Dirac points of graphene in the electronic structure of the heterostructure Graphene/1T-$CrTe_2$ are found to be tunable with an perpendicular external electric field, leading to the self-induced p-type or n-type doping effect.

3.3.8 Magnetoelectric coupling

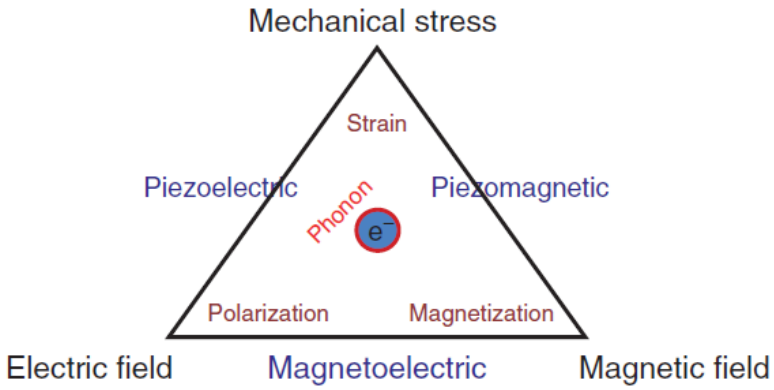

Figure 3.11: Schematic showing fields and coupling [42]

Magnetoelectric effect is the induction of magnetization with the application of an electric field or the induction of polarisation with the application of a magnetic field [43]. Since the electric field E and the magnetic field H are vectors, the coupling parameters will be tensors. Application of electric field leads to change in magnetization as shown in figure 3.12. The symmetry of a biferroic with both electrical and magnetic ordering naturally permits a nonzero magnetoelectric coupling. This can be understood by taking symmetry considerations for two order parameters, polarization P and magnetization M. Polarization is the electric dipole moment per unit volume and magnetization is the magnetic dipole moment per unit volume. In a quantum mechanical sense, polarization is equivalent to the expectation value of the position operator r, while magnetic moment corresponds to that of the angular momentum operator r x p (p is the momentum), which is related to the symmetry properties [42]. Under spatial and time inversion, it determines the transformation properties of P and M (under inversion i and reflection) are given as,

$$\begin{gathered} \hat{i}P = -P, \hat{i}M = M \\ \hat{\sigma_z}P_z = -P_z, \hat{\sigma_z}M_z = M_z \\ \hat{\sigma_z}P_x = P_x, \hat{\sigma_z}M_x = -M_x \end{gathered} \tag{3.4}$$

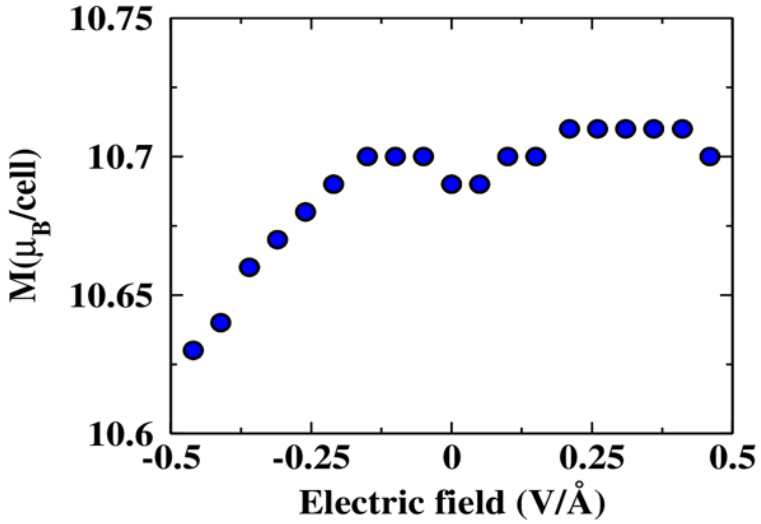

Figure 3.12: Variation of magnetization M under external electric field in the z-direction

From the theory discussed in section 1.3.1 of Chapter 1, the magnetoelectric coupling coefficient α_{ij} is calculated here as,

$$\alpha_{ij} = \mu_0 \frac{\partial M_i}{\partial E_j} \tag{3.5}$$

The above equation is applied to the negative electric field region, where linearity is observed. The magnetoelectric coupling coefficient α is equal to 0.804 psm^{-1}. Magnetoelectric coupling in heterostructure depends on the interplay among the spin and charge degrees of freedom across the interfaces.

3.3.9 Piezoelectricity and Piezomagnetism

The electronic, optical and magnetic properties can be tuned in 2D materials [44], especially semiconductors by applying an in-plane strain. The strain ε applied along a direction is defined as $\varepsilon = (l - l_o)/l_o$ x 100%, where l and l_o are the lattice constants of original and strained structure. Positive and negative signs indicate tensile and compressive strains respectively. Fig 7(a) shows variation of magnetization and polarization with biaxial strain applied along x and y-directions for relaxed structure of Graphene/1T-$CrTe_2$ vdW heterostructure, ranging from -1.5% to 1.5%.

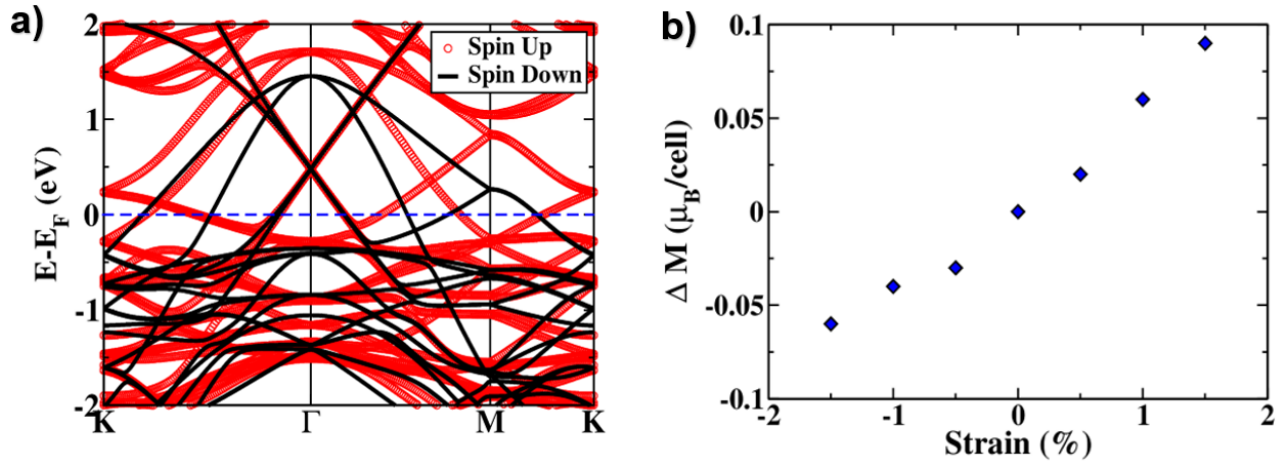

Figure 3.13: (a) Spin-resolved electronic structure of Graphene/1T-$CrTe_2$ under 0.5 % biaxial strain along x and y-directions (b) Change in magnetization under biaxial strains applied in the x and y-directions

Spin-resolved electronic structure is shown in figure 3.13(a), there is hardly any change in the electronic structure in comparison to that of unperturbed heterostructure. As shown in figure 3.13(b), with biaxial strains, there occurs small change in magnetization.

In figure 3.14, we concur that the magnetization of the heterostructure changes from 10.69 μ_B per cell to 10.75 μ_B per cell linearly with stress , which indicates that the in-plane biaxial strain, assumed to be isotropic, can affect the magnetization in the heterostructure. Consequently, there occurs a piezomagnetic effect. It is also interesting to observe that the polarization also changes linearly with stress. We calculated the linear piezoelectric and piezomagnetic coefficients d_{ij} and q_{ij} are given as

$$d_{ij} = \frac{\partial P}{\partial T} \tag{3.6}$$

$$q_{ij} = \frac{\partial M}{\partial T} \tag{3.7}$$

where T is the stress field and i, j indicates directions of polarization and applied stress, respectively. Fom above equations, estimate of piezoelectric coefficient d_{31} is 0.063 pm/V and piezomagnetic coefficient q_{31} is 16.32 pm/A. Consequently, strain applied to a heterostructure

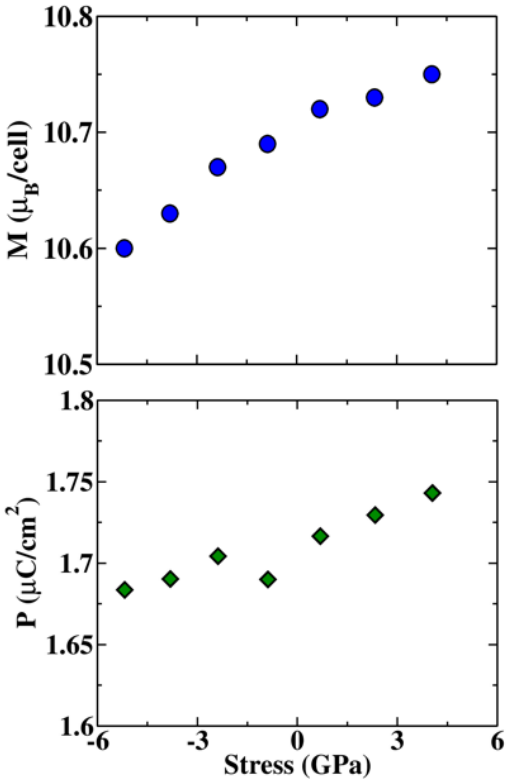

Figure 3.14: Magnetization M and polarization P as a function of stress in Graphene/1T-$CrTe_2$ heterostructure

changes its polarization and magnetization, which leads to appearance of piezoelectric and piezomagnetic effects.

3.3.10 Model of Dirac bands of graphene

To understand the gap opening up at the Dirac point of graphene at Γ point, we have developed the following model using k.p approximation. Electrons in a solid are described by the single electron Schrödinger equation given as

$$H\psi = (\frac{p^2}{2m} + V)\psi \tag{3.8}$$

where V is the periodic potential with symmetries that obey crystal's symmetry. The wave-function ψ follows Bloch's theorem expressed as,

$$\psi_{n,k}(x) = e^{ik.x} u_{n,k}(x) \tag{3.9}$$

where k is crystal momentum vector, n is band index and $u_{n.k}$ is periodic function having same periodicity as crystal. In each band, there is a relation between the wavevector k and the energy of the state E_n, k called the band dispersion [45].

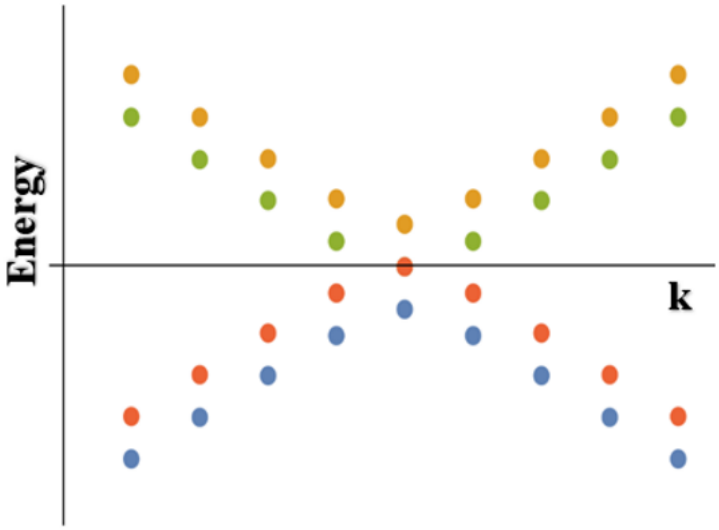

Figure 3.15: Energy dispersion of Dirac bands near Γ point within k.p approximation

The dirac bands hamiltonian (4x4) for a particular spin (up/down) can be reduced to 2 x 2 by making use of Pauli matrices σ_x, σ_y and σ_z expressed as,

$$\sigma_x = \begin{pmatrix} 0 & 1 \\ 1 & 0 \end{pmatrix}$$

$$\sigma_y = \begin{pmatrix} 0 & -i \\ i & 0 \end{pmatrix}$$

$$\sigma_z = \begin{pmatrix} 1 & 0 \\ 0 & -1 \end{pmatrix}$$

The four band hamiltonian can be written as,

$$H_{hetero} = \begin{pmatrix} \gamma_0 & \gamma_1 \\ \gamma_1 & \gamma_0 \end{pmatrix}$$

where γ_0 is the 2D Dirac hamiltonian of graphene is given by, $\gamma_0 = \hbar v_F \vec{\sigma}.\vec{k}$, where σ represents Pauli matrices, v_F is the Fermi velocity and $\vec{\sigma}.\vec{k}$=$k_x\sigma_x$+$k_y\sigma_y$.

$$\gamma_1 = \begin{pmatrix} d & 0 \\ 0 & 0 \end{pmatrix}$$

To model energy bands at Γ point as shown in figure 3.15, we have taken $k_y = 0$ and d = 0.02 to get energy dispersion within tight-binding approximation generated using Mathematica 12.0 (Wolfram Research).

3.4 Conclusions

Using first-principles calculations within density functional theory, we determine the electronic and magnetic properties of graphene/1T-$CrTe_2$ heterostructure. The negative binding energy of 160 meV/atom shows that fabircation of heterostructure is feasible. The results show that due to the magnetic proximity effect [41], there is spin splitting of graphene Dirac bands of 6.2 meV and 14 meV for spin up and spin down channels respectively, in the heterostructure. The Dirac points of graphene are shifted above the Fermi level due to electron transfer from graphene to 1T-$CrTe_2$ layer. Due to electron doping of heterostructure by one electron per two unit cells, the Dirac points of graphene shifts to the Fermi level and the energy difference between the Dirac bands increases to 18.4 meV and 22.8 meV for spin up and spin down respectively. The

Dirac points of graphene in the electronic structure of the heterostructure Graphene/1T-$CrTe_2$ shows tunability with an external electric field that results in the so-called self-induced p-type or n-type doping effect and are shifted to the Fermi level by one electron doping per two unit cells. The application of strain to the heterostructure ranging from -1.5% to 1.5% changes its polarization and magnetization, which leads to appearance of piezoelectric and piezomagnetic effects, with piezoelectric and piezomagnetic coefficients equal to 0.063 pm/V and 16.32 pm/A, respectively . Finally, the Dirac bands of graphene are modeled using k.p approximation.

Bibliography

[1] A. K. Geim and K. S. Novoselov, "The rise of graphene," in *Nanoscience and technology: a collection of reviews from nature journals*, pp. 11–19, World Scientific, 2010.

[2] M. Xu, T. Liang, M. Shi, and H. Chen, "Graphene-like two-dimensional materials," *Chemical reviews*, vol. 113, no. 5, pp. 3766–3798, 2013.

[3] A. C. Neto, F. Guinea, N. M. Peres, K. S. Novoselov, and A. K. Geim, "The electronic properties of graphene," *Reviews of modern physics*, vol. 81, no. 1, p. 109, 2009.

[4] L. Britnell, R. V. Gorbachev, R. Jalil, B. D. Belle, F. Schedin, M. I. Katsnelson, L. Eaves, S. V. Morozov, A. S. Mayorov, N. M. Peres, *et al.*, "Electron tunneling through ultrathin boron nitride crystalline barriers," *Nano letters*, vol. 12, no. 3, pp. 1707–1710, 2012.

[5] K. F. Mak, C. Lee, J. Hone, J. Shan, and T. F. Heinz, "Atomically thin mos 2: a new direct-gap semiconductor," *Physical review letters*, vol. 105, no. 13, p. 136805, 2010.

[6] X. Xi, Z. Wang, W. Zhao, J.-H. Park, K. T. Law, H. Berger, L. Forró, J. Shan, and K. F. Mak, "Ising pairing in superconducting nbse2 atomic layers," *Nature Physics*, vol. 12, no. 2, pp. 139–143, 2016.

[7] B. Huang, G. Clark, E. Navarro-Moratalla, D. R. Klein, R. Cheng, K. L. Seyler, D. Zhong, E. Schmidgall, M. A. McGuire, D. H. Cobden, *et al.*, "Layer-dependent ferromagnetism in a van der waals crystal down to the monolayer limit," *Nature*, vol. 546, no. 7657, pp. 270–273, 2017.

[8] S. Tang, C. Zhang, D. Wong, Z. Pedramrazi, H.-Z. Tsai, C. Jia, B. Moritz, M. Claassen, H. Ryu, S. Kahn, *et al.*, "Quantum spin hall state in monolayer 1t'-wte2," *Nature Physics*, vol. 13, no. 7, pp. 683–687, 2017.

[9] M. Bora and P. Deb, "Magnetic proximity effect in two-dimensional van der waals heterostructure," *Journal of Physics: Materials*, vol. 4, no. 3, p. 034014, 2021.

[10] K. S. Burch, D. Mandrus, and J.-G. Park, "Magnetism in two-dimensional van der waals materials," *Nature*, vol. 563, no. 7729, pp. 47–52, 2018.

[11] M. Yankowitz, Q. Ma, P. Jarillo-Herrero, and B. J. LeRoy, "van der waals heterostructures combining graphene and hexagonal boron nitride," *Nature Reviews Physics*, vol. 1, no. 2, pp. 112–125, 2019.

[12] P. Ajayan, P. Kim, and K. Banerjee, "van der waals materials," *Phys. Today*, vol. 69, no. 9, p. 38, 2016.

[13] P. Wei, S. Lee, F. Lemaitre, L. Pinel, D. Cutaia, W. Cha, F. Katmis, Y. Zhu, D. Heiman, J. Hone, *et al.*, "Strong interfacial exchange field in the graphene/eus heterostructure," *Nature materials*, vol. 15, no. 7, pp. 711–716, 2016.

[14] M. U. Farooq and J. Hong, "Switchable valley splitting by external electric field effect in graphene/cri3 heterostructures," *npj 2D Materials and Applications*, vol. 3, no. 1, pp. 1–7, 2019.

[15] S. K. Behera and P. Deb, "Controlling the bandgap in graphene/h-bn heterostructures to realize electron mobility for high performing fets," *RSC advances*, vol. 7, no. 50, pp. 31393–31400, 2017.

[16] A. Bano, J. Krishna, T. Maitra, and N. Gaur, "Cri3-wte2: A novel two-dimensional heterostructure as multisensor for brf3 and cocl2 toxic gases," *Scientific Reports*, vol. 9, no. 1, pp. 1–8, 2019.

[17] H.-D. Song, Y.-F. Wu, X. Yang, Z. Ren, X. Ke, M. Kurttepeli, G. V. Tendeloo, D. Liu, H.-C. Wu, B. Yan, *et al.*, "Asymmetric modulation on exchange field in a graphene/bifeo3 heterostructure by external magnetic field," *Nano letters*, vol. 18, no. 4, pp. 2435–2441, 2018.

[18] Z. Fei, B. Huang, P. Malinowski, W. Wang, T. Song, J. Sanchez, W. Yao, D. Xiao, X. Zhu, A. F. May, *et al.*, "Two-dimensional itinerant ferromagnetism in atomically thin fe3gete2," *Nature materials*, vol. 17, no. 9, pp. 778–782, 2018.

[19] D. J. O'Hara, T. Zhu, A. H. Trout, A. S. Ahmed, Y. K. Luo, C. H. Lee, M. R. Brenner, S. Rajan, J. A. Gupta, D. W. McComb, *et al.*, "Room temperature intrinsic ferromagnetism in epitaxial manganese selenide films in the monolayer limit," *Nano letters*, vol. 18, no. 5, pp. 3125–3131, 2018.

[20] M. Bonilla, S. Kolekar, Y. Ma, H. C. Diaz, V. Kalappattil, R. Das, T. Eggers, H. R. Gutierrez, M.-H. Phan, and M. Batzill, "Strong room-temperature ferromagnetism in vse2 monolayers on van der waals substrates," *Nature nanotechnology*, vol. 13, no. 4, pp. 289–293, 2018.

[21] J. Chen, Y. Shan, Q. Wang, J. Zhu, and R. Liu, "P-type laser-doped wse2/mote2 van der waals heterostructure photodetector," *Nanotechnology*, vol. 31, no. 29, p. 295201, 2020.

[22] A. Purbawati, J. Coraux, J. Vogel, A. Hadj-Azzem, N. J. Wu, N. Bendiab, D. Jegouso, J. Renard, L. Marty, V. Bouchiat, A. Sulpice, L. Aballe, M. Foerster, F. Genuzio, A. Locatelli, T. O. Menteş, Z. V. Han, X. Sun, M. Núñez-Regueiro, and N. Rougemaille, "In-plane magnetic domains and neél-like domain walls in thin flakes of the room temperature crte2van der waals ferromagnet," *ACS Applied Materials and Interfaces*, vol. 12, pp. 30702–30710, 7 2020.

[23] X. Sun, W. Li, X. Wang, Q. Sui, T. Zhang, Z. Wang, L. Liu, D. Li, S. Feng, S. Zhong, *et al.*, "Room temperature ferromagnetism in ultra-thin van der waals crystals of 1t-crte2," *Nano Research*, vol. 13, no. 12, pp. 3358–3363, 2020.

[24] D. C. Freitas, R. Weht, A. Sulpice, G. Remenyi, P. Strobel, F. Gay, J. Marcus, and M. Núñez-Regueiro, "Ferromagnetism in layered metastable 1t-crte2," *Journal of Physics Condensed Matter*, vol. 27, 5 2015.

[25] A. Otero Fumega, J. Phillips, and V. Pardo, "Controlled two-dimensional ferromagnetism in 1t–crte2: the role of charge density wave and strain," *The Journal of Physical Chemistry C*, vol. 124, no. 38, pp. 21047–21053, 2020.

[26] J. P. Perdew, K. Burke, and M. Ernzerhof, "Generalized gradient approximation made simple," *Physical review letters*, vol. 77, no. 18, p. 3865, 1996.

[27] P. Giannozzi, S. Baroni, N. Bonini, M. Calandra, R. Car, C. Cavazzoni, D. Ceresoli, G. L. Chiarotti, M. Cococcioni, I. Dabo, *et al.*, "Quantum espresso: a modular and open-source software project for quantum simulations of materials," *Journal of physics: Condensed matter*, vol. 21, no. 39, p. 395502, 2009.

[28] G. Kresse and D. Joubert, "From ultrasoft pseudopotentials to the projector augmented-wave method," *Physical review b*, vol. 59, no. 3, p. 1758, 1999.

[29] J. J. Mortensen, L. B. Hansen, and K. W. Jacobsen, "Real-space grid implementation of the projector augmented wave method," *Physical Review B*, vol. 71, no. 3, p. 035109, 2005.

[30] S. Grimme, "Semiempirical gga-type density functional constructed with a long-range dispersion correction," *Journal of computational chemistry*, vol. 27, no. 15, pp. 1787–1799, 2006.

[31] V. I. Anisimov, I. Solovyev, M. Korotin, M. Czyżyk, and G. Sawatzky, "Density-functional theory and nio photoemission spectra," *Physical Review B*, vol. 48, no. 23, p. 16929, 1993.

[32] A. Liechtenstein, V. I. Anisimov, and J. Zaanen, "Density-functional theory and strong interactions: Orbital ordering in mott-hubbard insulators," *Physical Review B*, vol. 52, no. 8, p. R5467, 1995.

[33] S. Li, S.-S. Wang, B. Tai, W. Wu, B. Xiang, X.-L. Sheng, and S. A. Yang, "Tunable anomalous hall transport in bulk and two-dimensional 1 t- crte 2: A first-principles study," *Physical Review B*, vol. 103, no. 4, p. 045114, 2021.

[34] H. J. Monkhorst and J. D. Pack, "Special points for brillouin-zone integrations," *Physical review B*, vol. 13, no. 12, p. 5188, 1976.

[35] K. Lasek, P. M. Coelho, K. Zberecki, Y. Xin, S. K. Kolekar, J. Li, and M. Batzill, "Molecular beam epitaxy of transition metal (ti-, v-, and cr-) tellurides: from monolayer ditellurides to multilayer self-intercalation compounds," *ACS nano*, vol. 14, no. 7, pp. 8473–8484, 2020.

[36] W. Setyawan and S. Curtarolo, "High-throughput electronic band structure calculations: Challenges and tools," *Computational materials science*, vol. 49, no. 2, pp. 299–312, 2010.

[37] S. Wang, J.-P. Chou, C. Ren, H. Tian, J. Yu, C. Sun, Y. Xu, and M. Sun, "Tunable schottky barrier in graphene/graphene-like germanium carbide van der waals heterostructure," *Scientific reports*, vol. 9, no. 1, pp. 1–7, 2019.

[38] Y. C. Zhou, H. L. Zhang, and W. Q. Deng, "A 3n rule for the electronic properties of doped graphene," *Nanotechnology*, vol. 24, 6 2013.

[39] S. K. Behera, M. Bora, S. S. P. Chowdhury, and P. Deb, "Proximity effects in graphene and ferromagnetic crbr 3 van der waals heterostructures," *Physical Chemistry Chemical Physics*, vol. 21, no. 46, pp. 25788–25796, 2019.

[40] I. E. Dzyaloshinskii, "On the magneto-electrical effects in antiferromagnets," *Soviet Physics JETP*, vol. 10, pp. 628–629, 1960.

[41] M. Fiebig, "Revival of the magnetoelectric effect," *Journal of physics D: applied physics*, vol. 38, no. 8, p. R123, 2005.

[42] U. V. Waghmare, "Multiferroics with magnetoelectric coupling," *Functional Metal Oxides: New Science and Novel Applications*, pp. 267–283, 2013.

[43] G. Lawes and G. Srinivasan, "Introduction to magnetoelectric coupling and multiferroic films," *Journal of Physics D: Applied Physics*, vol. 44, no. 24, p. 243001, 2011.

[44] W. Wu, L. Wang, Y. Li, F. Zhang, L. Lin, S. Niu, D. Chenet, X. Zhang, Y. Hao, T. F. Heinz, *et al.*, "Piezoelectricity of single-atomic-layer mos2 for energy conversion and piezotronics," *Nature*, vol. 514, no. 7523, pp. 470–474, 2014.

[45] C. Kittel and P. McEuen, *Kittel's Introduction to Solid State Physics*. John Wiley & Sons, 2018.

Chapter 4

Summary

The central theme of this thesis is to explore electronic and magnetic properties of heterostructure created by stacking graphene of 3x3 supercell over 1T-$CrTe_2$ monolayer of 2x2 supercell, which is reported to be 2D magnetic material showing ferromagnetism at room temperature. The heterostructure is constructed having lattice mismatch of 0.54%. The heterostructure The electronic structure showed that the heterostructure has metallic character and that the Dirac points of graphene shoft above the Fermi level by 6.2 meV and 14 meV for spin up and spin down channels, respectively. This shift is accounted by the electron transfer from graphene layer to 1T-$CrTe_2$ layer. The Dirac points of graphene are tunable with respect to perturbations applied such as perpendicular electric field in z-direction, carrier doping (holes and electrons) and biaxial strain in x and y-directions. We found some interesting effects such as magnetoelectric effect, piezoelectric effect and piezomagnetic effect. With application of external electric field in z-direction, the Dirac points of graphene tune with positive and negative electric field. Because of electron doping of the heterostructure by one electron per two unit cell, the Dirac points of graphene shifts to the Fermi level and the energy difference between the Dirac bands increases to 18.4 meV and 22.8 meV for spin up and spin down respectively. Similar shift of the Dirac points of graphene to the Fermi level is seen with application of negative electric field of 0.26 V/Åalong z-direction. The polarization and magnetization in the heterostructure varies with

external electric field, carrier doping and application of stress. The magnetoelectric effect is prevalent in the heterostructure, with a non-zero magnetoelectric coupling coefficient of 0.804 ps/m. The heterostructure exhibits piezoelectricity and piezomagnetism. The piezoelectric and piezomagnetic coefficients are calculated to be 0.063 pm/V and 16.32 pm/A, respectively. Our work can serve as a foundation for understanding graphene based vdW heterostructures.